Numerical Accuracy in Solutions of the Shallow-Water Equations

Preliminary Report

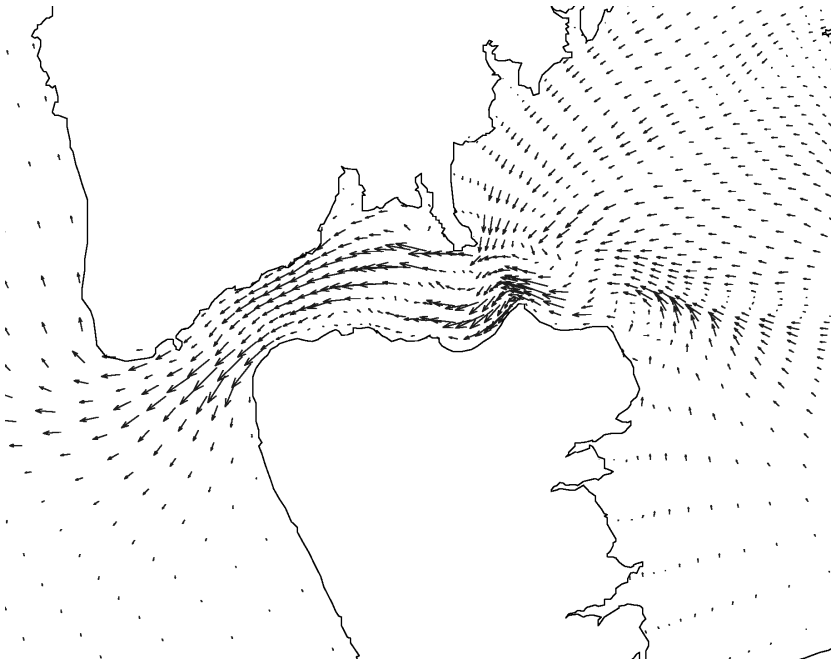

Peterjan Broomans

Delft, July 2002

TU Delft & WL | Delft Hydraulics
supervisors: Prof.dr.ir. P. Wesseling
Dr.ir. C. Vuik
Prof.dr.ir. A.E. Mynett
Ir. J. Mooiman

Contents

List of symbols

symbol	*description*	*unit*
d	water depth with respect to a reference level	$[m]$
f	Coriolis parameter	$[1/s]$
f_x	Coriolis force component in x-direction (per unit mass)	$[m/s^2]$
f_y	Coriolis force component in y-direction (per unit mass)	$[m/s^2]$
f_z	Coriolis force component in z-direction (per unit mass)	$[m/s^2]$
g	gravitational acceleration	$[m/s^2]$
H	total water depth ($\zeta + d$)	$[m]$
k	turbulent kinetic energy	$[m^2/s^2]$
l_m	mixing length	$[m]$
p	pressure	$[kg/(ms^2)]$
$\bar{p}$	time-averaged pressure	$[kg/(ms^2)]$
p_a	atmospheric pressure	$[kg/(ms^2)]$
u	flow velocity component in x-direction	$[m/s]$
$\bar{u}$	time-averaged flow velocity component in x-direction	$[m/s]$
U	depth-averaged flow velocity component in x-direction	$[m/s]$
v	flow velocity component in y-direction	$[m/s]$
$\bar{v}$	time-averaged flow velocity component in y-direction	$[m/s]$
V	depth-averaged flow velocity component in y-direction	$[m/s]$
w	flow velocity component in z-direction	$[m/s]$
$\bar{w}$	time-averaged flow velocity component in z-direction	$[m/s]$
α_ζ	'reflection coefficient' (water level boundary)	$[s^2]$
α_U	'reflection coefficient' (velocity boundary)	$[s]$
ϵ	dissipation rate of turbulent kinetic energy	$[m^2/s^3]$
ζ	free surface elevation with respect to a reference level	$[m]$
κ	Von Kármán constant	[-]
ν	kinematic viscosity	$[m^2/s]$
ν_t	eddy viscosity	$[m^2/s]$
ν_t^{2D}	part of horizontal eddy viscosity due to "2D turbulence"	$[m^2/s]$
ν_t^H	horizontal eddy viscosity	$[m^2/s]$
ν_t^V	vertical eddy viscosity	$[m^2/s]$
ρ	density	$[kg/m^3]$
ρ_0	reference density	$[kg/m^3]$
σ	transformed vertical coordinate	[-]
τ	time step	$[s]$
τ_{bx}	bed shear stress in x-direction	$[1/(ms)]$
τ_{by}	bed shear stress in y-direction	$[1/(ms)]$
$\vec{\tau}_s$	wind stress	$[1/(ms)]$
ϕ	geophysical latitude	[-]
Ω	angular speed of the earth	$[1/s]$
$\underline{\Omega}$	rotation vector of the earth	$[1/s]$
ω	transformed vertical flow velocity component	$[m/s]$

1 Introduction

The computer program Delft3D-FLOW can be used to compute a numerical approximation of the solution of the shallow-water equations. The shallow-water equations describe the flow of water in rivers, lakes and shallow seas, like the North Sea. The result of a Delft3D-FLOW simulation can be used to solve the transport equations for some contaminant or to determine whether dykes along a river need to be heightened.

The solution obtained by Delft3D-FLOW is the product of a modelling process subject to uncertainties and errors (AIAA, 1998), see Figure 1. The first step in this process is the derivation of the shallow-water equations, which comprise a physical model for the natural water flows. Lack of knowledge on the physical aspects (turbulence, boundary conditions) in this step is the general cause of uncertainty within the modelling process. This may be the cause of the difference between experimental and computational data (Oberkampf and Blottner, 1998). Uncertainty will not be dealt with in this report.

The analytical (i.e. exact) solution of the shallow-water equations can not be determined, so an approximation will have to be calculated. The next step in the modelling process is the construction of a numerical model for the shallow-water equations. During this construction truncation errors are made. When solving the numerical model small errors, like rounding errors and iteration errors, are unavoidable. To a certain extent it is possible to calculate an upper bound for these errors.

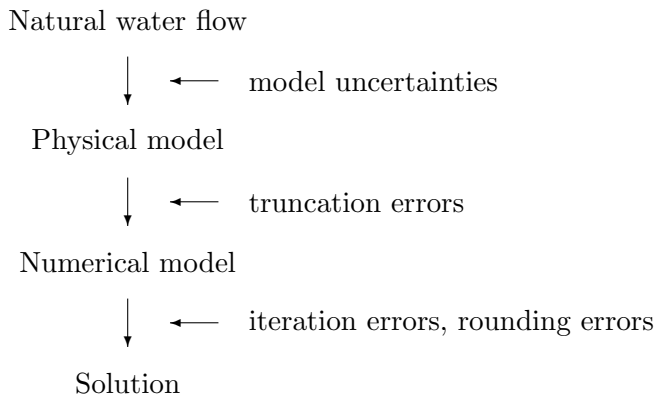

Figure 1. Uncertainties and errors in the various steps of the solution process.

The aim of this research is to track down, explain and quantify numerical errors in Delft3D-FLOW and, if necessary, find solutions to reduce these errors. For this purpose several test cases will be set up, which show erroneous results. Then the computations which cause these errors will have to be located, so the errors can be evaluated. Finally, a solution will be suggested and tested.

In the second chapter the shallow-water equations will be derived and their boundary conditions will be discussed. The third chapter focuses on the staggered grid, the numerical scheme and the procedure for solving the numerical equations. In the fourth chapter test cases are stated and illustrated.

2 Flow model

The Navier-Stokes equations are a general model which can be used to model water flows in many applications. However, when considering a problem in which the horizontal scale is much larger than the vertical one the three-dimensional shallow-water equations will suffice.

First we will derive the Reynolds-averaged Navier-Stokes equations describing turbulent flows for which the length scale of the turbulence is much smaller than that of the problem. Then we will derive the three-dimensional shallow-water equations under the assumption that the pressure is hydrostatically distributed. These equations will be transformed to σ-coordinates, after which the boundary conditions and the turbulence modelling will be discussed.

2.1 Reynolds-averaged Navier-Stokes equations

The Navier-Stokes equations are given by

$$\begin{aligned}
\frac{\partial u}{\partial t} + u\frac{\partial u}{\partial x} + v\frac{\partial u}{\partial y} + w\frac{\partial u}{\partial z} &= -\frac{1}{\rho_0}\frac{\partial p}{\partial x} + \nu\triangle u - f_x \\
\frac{\partial v}{\partial t} + u\frac{\partial v}{\partial x} + v\frac{\partial v}{\partial y} + w\frac{\partial v}{\partial z} &= -\frac{1}{\rho_0}\frac{\partial p}{\partial y} + \nu\triangle v - f_y \\
\frac{\partial w}{\partial t} + u\frac{\partial w}{\partial x} + v\frac{\partial w}{\partial y} + w\frac{\partial w}{\partial z} &= -\frac{1}{\rho_0}\frac{\partial p}{\partial z} + \nu\triangle w - f_z - \frac{\rho}{\rho_0}g,
\end{aligned} \tag{1}$$

where u, v and w denote the velocity components in the x-, y- and z-direction respectively, ρ the density, ρ_0 the reference density, p the pressure, ν the kinematic viscosity and f_x, f_y and f_z represent the components of the Coriolis forces per unit mass. They are defined by $(f_x, f_y, f_z)^T = -2\underline{\Omega} \times (u, v, w)^T$, where $\underline{\Omega}$ is the earth's rotation vector. The Navier-Stokes equations in (1) are valid under the assumption that the density is constant or if the Boussinesq approximation applies.

Assumption 1 (Boussinesq approximation). *The Boussinesq approximation states that if density variations are small the density may be assumed constant in all terms except the gravitational term.*

Due to turbulence eddies small variations occur in the flow velocities and pressure. Usually these variations are too small to be represented in a numerical scheme unless the grid is chosen very fine. To deal with this phenomenon we first decompose the velocities and the pressure as follows

$$u = \bar{u} + u', \quad v = \bar{v} + v', \quad w = \bar{w} + w' \quad \text{and} \quad p = \bar{p} + p', \tag{2}$$

where the overbar represents time-averaged quantities. For instance $\bar{u}$ is defined by

$$\bar{u}(t) := \frac{1}{T}\int_t^{t+T} u(\tau)d\tau.$$

The period T should be larger than the turbulence time scale, but smaller than long periodic effects such as the tidal scale. The turbulent fluctuations are given by u', v', w' and p'. Note that the time-averages of these fluctuations are zero, i.e. $\frac{1}{T}\int_t^{t+T} u'\, d\tau = 0$.

When substituting (2) into (1) and averaging the resulting equations over time the Reynolds-averaged Navier-Stokes equations or simply Reynolds equations arise for turbulent flows. They

read

$$\frac{\partial \bar{u}}{\partial t} + \bar{u}\frac{\partial \bar{u}}{\partial x} + \bar{v}\frac{\partial \bar{u}}{\partial y} + \bar{w}\frac{\partial \bar{u}}{\partial z} + \frac{\partial \overline{u'u'}}{\partial x} + \frac{\partial \overline{u'v'}}{\partial y} + \frac{\partial \overline{u'w'}}{\partial z} = -\frac{1}{\rho_0}\frac{\partial \bar{p}}{\partial x} - \bar{f}_x \tag{3a}$$

$$\frac{\partial \bar{v}}{\partial t} + \bar{u}\frac{\partial \bar{v}}{\partial x} + \bar{v}\frac{\partial \bar{v}}{\partial y} + \bar{w}\frac{\partial \bar{v}}{\partial z} + \frac{\partial \overline{v'u'}}{\partial x} + \frac{\partial \overline{v'v'}}{\partial y} + \frac{\partial \overline{v'w'}}{\partial z} = -\frac{1}{\rho_0}\frac{\partial \bar{p}}{\partial y} - \bar{f}_y \tag{3b}$$

$$\frac{\partial \bar{w}}{\partial t} + \bar{u}\frac{\partial \bar{w}}{\partial x} + \bar{v}\frac{\partial \bar{w}}{\partial y} + \bar{w}\frac{\partial \bar{w}}{\partial z} + \frac{\partial \overline{w'u'}}{\partial x} + \frac{\partial \overline{w'v'}}{\partial y} + \frac{\partial \overline{w'w'}}{\partial z} = -\frac{1}{\rho_0}\frac{\partial \bar{p}}{\partial z} - \bar{f}_z - \frac{\rho}{\rho_0}g. \tag{3c}$$

The correlations between fluctuating velocity components ($\overline{u'u'}$, $\overline{u'v'}$, etc.) are unknown. These correlations are responsible for a loss of momentum in the mean flow direction and therefore appear to act as stresses on the fluid. They are called Reynolds stresses. These stresses are much larger than the viscous stresses which have therefore been neglected.

Assumption 2 (Eddy viscosity concept or Boussinesq hypothesis). *Reynolds stresses like viscous stresses depend on the deformation of the mean flow. Thus, the Reynolds stresses are modelled as*

$$\overline{u'v'} = -\nu_t \left(\frac{\partial \bar{v}}{\partial x} + \frac{\partial \bar{u}}{\partial y} \right), \tag{4}$$

where ν_t is the so-called eddy viscosity. This eddy viscosity is a priori unknown and a suitable expression has to be constructed (see section 2.5).

2.2 Three-dimensional shallow-water equations

We speak of shallow water only when a flow satisfies certain characteristic relations.

Assumption 3 (Shallow water). *(i) The characteristic horizontal length scale is much larger than the characteristic vertical length scale. (ii) The characteristic vertical velocity is small in comparison with the characteristic horizontal velocity (Jin, 1993).*

These assumptions allow that the terms $\frac{\partial \bar{w}}{\partial x}$ and $\frac{\partial \bar{w}}{\partial y}$ are neglected. Also the difference between the horizontal and the vertical length scale justifies a distinction between a horizontal (ν_t^H) and a vertical (ν_t^V) eddy viscosity. But more importantly, the momentum equation in the vertical direction reduces to the hydrostatic pressure distribution

$$\frac{\partial \bar{p}}{\partial z} = -\rho g. \tag{5}$$

Integrating this equation results in

$$\bar{p}(x, y, z, t) = g \int_z^\zeta \rho \, dz + p_a, \tag{6}$$

where $\zeta = \zeta(x, y, t)$ is the free surface level against the reference plane $z = 0$ and p_a is the atmospheric pressure. Substituting this result in the pressure term of (3a) and using Leibnitz' integration rule, yields

$$-\frac{1}{\rho_0}\frac{\partial \bar{p}}{\partial x} = -\frac{\rho g}{\rho_0}\frac{\partial \zeta}{\partial x} - \frac{g}{\rho_0}\int_z^\zeta \frac{\partial \rho}{\partial x}\, dz' - \frac{1}{\rho_0}\frac{\partial p_a}{\partial x}.$$

The horizontal pressure gradient is described by differences of the water level ζ through the barotropic term, the first term on the right-hand-side, and by density differences in horizontal direction through the baroclinic term, the second term. The last term on the right-hand side

describes the contribution of the atmospheric pressure. If we had taken ρ constant, (6) would read $\bar{p} = \rho g(\zeta - z) + p_a$ and for the pressure term of (3a) we would have

$$-\frac{1}{\rho_0}\frac{\partial \bar{p}}{\partial x} = -g\frac{\partial \zeta}{\partial x} - \frac{1}{\rho_0}\frac{\partial p_a}{\partial x}.$$

From this point on we will consider the density constant and neglect the atmospheric pressure gradient. Note that in Delft3D-FLOW these simplifications are not carried through.

Substituting equations (4) and (6) in equations (3a) and (3b) yields, dropping the overbar,

$$\begin{aligned}\frac{\partial u}{\partial t} + u\frac{\partial u}{\partial x} + v\frac{\partial u}{\partial y} + w\frac{\partial u}{\partial z} &= -g\frac{\partial \zeta}{\partial x} + fv \\ &+ 2\frac{\partial}{\partial x}\left(\nu_t^H \frac{\partial u}{\partial x}\right) + \frac{\partial}{\partial y}\left(\nu_t^H\left(\frac{\partial u}{\partial y} + \frac{\partial v}{\partial x}\right)\right) + \frac{\partial}{\partial z}\left(\nu_t^V \frac{\partial u}{\partial z}\right)\end{aligned} \tag{7}$$

and

$$\begin{aligned}\frac{\partial v}{\partial t} + u\frac{\partial v}{\partial x} + v\frac{\partial v}{\partial y} + w\frac{\partial v}{\partial z} &= -g\frac{\partial \zeta}{\partial y} - fu \\ &+ \frac{\partial}{\partial x}\left(\nu_t^H\left(\frac{\partial u}{\partial y} + \frac{\partial v}{\partial x}\right)\right) + 2\frac{\partial}{\partial y}\left(\nu_t^H \frac{\partial v}{\partial y}\right) + \frac{\partial}{\partial z}\left(\nu_t^V \frac{\partial v}{\partial z}\right),\end{aligned} \tag{8}$$

where f, the Coriolis parameter, is defined by

$$f = 2\Omega \sin\phi$$

with Ω the angular speed of the earth and ϕ the latitude. The equations (7), (8) and the incompressible continuity equation

$$\frac{\partial u}{\partial x} + \frac{\partial v}{\partial y} + \frac{\partial w}{\partial z} = 0 \tag{9}$$

are called the shallow-water equations. Together with initial and boundary conditions they can be used to compute the flow velocity components.

Integrating the continuity equation along the vertical axis results in

$$w(x, y, \zeta, t) - w(x, y, d, t) = -\int_{-d}^{\zeta} \frac{\partial u}{\partial x}\, dz - \int_{-d}^{\zeta} \frac{\partial v}{\partial y}\, dz, \tag{10}$$

where $d = d(x, y)$ is the water depth below the reference plane $z = 0$. Morphological changes of the bed due to the water flow are in general very small and they are therefore neglected. Thus d is not dependent on the time. Equation (10) can be rewritten by using substitutions for w at the bottom and the water surface. For $z = \zeta(x, y, t)$ we have

$$w = \frac{d\zeta}{dt} = \frac{\partial \zeta}{\partial t} + u\frac{\partial \zeta}{\partial x} + v\frac{\partial \zeta}{\partial y}. \tag{11}$$

A similar condition at the bottom reads

$$w = -u\frac{\partial d}{\partial x} - v\frac{\partial d}{\partial y}. \tag{12}$$

Substituting (11) and (12) into (10) and using Leibnitz' integration rule, yields

$$\frac{\partial \zeta}{\partial t} = -\frac{\partial}{\partial x}\int_{-d}^{\zeta} u\, dz - \frac{\partial}{\partial y}\int_{-d}^{\zeta} v\, dz. \tag{13}$$

2.3 Transformed equations in σ-coordinates

The bottom and the water surface are usually not parallel to the reference plane ($z = 0$). In order to cope with uneven bottom topographies in numerical applications a transformation is applied to so-called σ-coordinates (Phillips, 1957). This transformation stretches the vertical direction, such that the transformed water depth is constant in space and time. The σ-coordinates are defined by

$$\tilde{x} = x, \quad \tilde{y} = y, \quad \sigma = \frac{z - \zeta}{H}, \quad \tilde{t} = t,$$

where $H = H(x, y, t) = \zeta + d$ is the water depth. The time-derivative in σ-coordinates reads

$$\frac{\partial}{\partial t} = \frac{\partial}{\partial \tilde{t}} + \frac{\partial \sigma}{\partial \tilde{t}} \frac{\partial}{\partial \sigma}.$$

For the spatial derivatives in the horizontal directions similar expressions hold. In the vertical direction we have

$$\frac{\partial}{\partial z} = \frac{1}{H} \frac{\partial}{\partial \sigma}.$$

The hydrostatic pressure relation (5) after transforming to σ-coordinates and integrating along the vertical axis, reads

$$\tilde{p} = p_a + gH \int_{\sigma}^{0} \rho(\tilde{x}, \tilde{y}, \sigma', \tilde{t}) \, d\sigma'. \tag{14}$$

The transformed vertical velocity is defined by

$$\begin{aligned} \omega := H \frac{\mathrm{D}\sigma}{\mathrm{D}\tilde{t}} &= H \left[\frac{\partial}{\partial t} \left(\frac{z - \zeta}{H} \right) + u \frac{\partial}{\partial x} \left(\frac{z - \zeta}{H} \right) + v \frac{\partial}{\partial y} \left(\frac{z - \zeta}{H} \right) \right] \\ &= w - \left(\frac{\partial \zeta}{\partial t} + u \frac{\partial \zeta}{\partial x} + v \frac{\partial \zeta}{\partial y} \right) - \sigma \left(\frac{\partial H}{\partial t} + u \frac{\partial H}{\partial x} + v \frac{\partial H}{\partial y} \right). \end{aligned} \tag{15}$$

The horizontal velocities u and v remain strictly horizontal after the transformation. Hence $\tilde{u} = u$ and $\tilde{v} = v$. When we use equation (15) on equation (9), noting that H and ζ are not dependent on σ, but $\tilde{u}$ and $\tilde{v}$ are, and assuming that d is not time-dependent, we obtain the continuity equation in transformed coordinates:

$$\frac{\partial \zeta}{\partial \tilde{t}} + \frac{\partial H\tilde{u}}{\partial \tilde{x}} + \frac{\partial H\tilde{v}}{\partial \tilde{y}} + \frac{\partial \omega}{\partial \sigma} = 0. \tag{16}$$

Integrating equation (16) from the bottom to the surface and using Leibnitz' integration rule, yields

$$\frac{\partial \zeta}{\partial \tilde{t}} + \frac{\partial HU}{\partial \tilde{x}} + \frac{\partial HV}{\partial \tilde{y}} = 0, \tag{17}$$

where U and V are depth-averaged velocities defined by $U = \int_{-1}^{0} \tilde{u} \, d\sigma$ and $V = \int_{-1}^{0} \tilde{v} \, d\sigma$.

The momentum equations in x- and y-direction in σ-coordinates are, dropping the tilde,

$$\frac{\partial u}{\partial t} + u \frac{\partial u}{\partial x} + v \frac{\partial u}{\partial y} + \frac{\omega}{H} \frac{\partial u}{\partial \sigma} = -\frac{1}{\rho_0} \left(\frac{\partial p}{\partial x} + \frac{\partial \sigma}{\partial x} \frac{\partial p}{\partial \sigma} \right) + fv + F_x + \frac{1}{H^2} \frac{\partial}{\partial \sigma} \left(\nu_t^V \frac{\partial u}{\partial \sigma} \right) \tag{18}$$

and

$$\frac{\partial v}{\partial t} + u \frac{\partial v}{\partial x} + v \frac{\partial v}{\partial y} + \frac{\omega}{H} \frac{\partial v}{\partial \sigma} = -\frac{1}{\rho_0} \left(\frac{\partial p}{\partial y} + \frac{\partial \sigma}{\partial y} \frac{\partial p}{\partial \sigma} \right) - fu + F_y + \frac{1}{H^2} \frac{\partial}{\partial \sigma} \left(\nu_t^V \frac{\partial v}{\partial \sigma} \right). \tag{19}$$

The terms F_x and F_y represent the horizontal viscosity terms. They are given by

$$F_x = \left(\frac{\partial}{\partial x} + \frac{\partial \sigma}{\partial x}\frac{\partial}{\partial \sigma}\right)\tau_{xx} + \left(\frac{\partial}{\partial y} + \frac{\partial \sigma}{\partial y}\frac{\partial}{\partial \sigma}\right)\tau_{xy}$$

and

$$F_y = \left(\frac{\partial}{\partial x} + \frac{\partial \sigma}{\partial x}\frac{\partial}{\partial \sigma}\right)\tau_{xy} + \left(\frac{\partial}{\partial y} + \frac{\partial \sigma}{\partial y}\frac{\partial}{\partial \sigma}\right)\tau_{yy},$$

where the Reynolds stresses τ_{xx}, τ_{xy} and τ_{yy} satisfy

$$\begin{aligned}
\tau_{xx} &= 2\nu_t^H \left(\frac{\partial u}{\partial x} + \frac{\partial \sigma}{\partial x}\frac{\partial u}{\partial \sigma}\right) \\
\tau_{xy} &= \nu_t^H \left(\frac{\partial u}{\partial y} + \frac{\partial \sigma}{\partial y}\frac{\partial u}{\partial \sigma} + \frac{\partial v}{\partial x} + \frac{\partial \sigma}{\partial x}\frac{\partial v}{\partial \sigma}\right) \\
\tau_{yy} &= 2\nu_t^H \left(\frac{\partial v}{\partial y} + \frac{\partial \sigma}{\partial y}\frac{\partial v}{\partial \sigma}\right).
\end{aligned}$$

For large scale problems with coarse horizontal grids, i.e. when shear-stresses along the boundaries may be neglected, the forces F_x and F_y may be simplified. First the horizontal eddy viscosity ν_t^H is assumed constant and then the horizontal eddy viscosity terms are reduced to the Laplace operator:

$$F_x = \nu_t^H \triangle u \quad \text{and} \quad F_y = \nu_t^H \triangle v \tag{20}$$

with $\triangle = \frac{\partial^2}{\partial x^2} + \frac{\partial^2}{\partial y^2}$. After application of this simplification we allow the horizontal eddy viscosity to vary in space.

Finally we will look at the horizontal pressure gradient in σ-coordinates, which can be written as

$$\frac{\partial p}{\partial x} + \frac{\partial \sigma}{\partial x}\frac{\partial p}{\partial \sigma} = \frac{\partial p}{\partial x} - \frac{1}{H}\left(\frac{\partial \zeta}{\partial x} + \sigma\frac{\partial H}{\partial x}\right)\frac{\partial p}{\partial \sigma}.$$

Substituting the integrated hydrostatic pressure relation (14) results in

$$\frac{\partial p_a}{\partial x} + g\frac{\partial}{\partial x}\left(H\int_\sigma^0 \rho\, d\sigma'\right) + g\rho\left(\frac{\partial \zeta}{\partial x} + \sigma\frac{\partial H}{\partial x}\right).$$

This expression has been implemented in Delft3D-FLOW. If we take the density constant and neglect the atmospheric pressure gradient, the horizontal pressure gradient reduces to the barotropic term $g\rho\frac{\partial \zeta}{\partial x}$ as shown before in the previous section.

2.4 Boundary conditions

Due to the impermeability of the surface and the bottom the following conditions apply:

$$\omega|_{\sigma=-1} = \omega|_{\sigma=0} = 0.$$

By imposing these conditions we neglect evaporation, rainfall and exchange with the ground water. At the sea bed the boundary conditions for the momentum equations are given by

$$\left.\frac{\nu_t^V}{H}\frac{\partial u}{\partial \sigma}\right|_{\sigma=-1} = \frac{1}{\rho}\tau_{bx} \tag{21}$$

and

$$\left.\frac{\nu_t^V}{H}\frac{\partial v}{\partial \sigma}\right|_{\sigma=-1} = \frac{1}{\rho}\tau_{by} \tag{22}$$

with τ_{bx} and τ_{by} the components of the bed shear stress in x- and y-direction, respectively.

Wind stresses are responsible for non-homogeneous boundary conditions for the momentum equations at the free surface. They read

$$\left.\frac{\nu_t^V}{H}\frac{\partial u}{\partial \sigma}\right|_{\sigma=0} = \frac{1}{\rho}\,|\vec{\tau}_s|\cos\theta \tag{23}$$

and

$$\left.\frac{\nu_t^V}{H}\frac{\partial v}{\partial \sigma}\right|_{\sigma=0} = \frac{1}{\rho}\,|\vec{\tau}_s|\sin\theta \tag{24}$$

with $|\vec{\tau}_s|$ the wind stress and θ the angle between the wind stress vector and x-axis.

Assumption 4 (Wind stress). *The expression for the wind stress is*

$$|\vec{\tau}_s| = \rho_a C_d U_{10}^2$$

where ρ_a is the air density, U_{10} is the wind speed 10 metres above the water surface and C_d is the wind drag coefficient, which depends on U_{10}.

This dependence is empirical and several implementations are possible, for example a linear relation, a constant value for C_d or a combination of the two.

The conditions at the vertical boundary planes are divided in open and closed boundary conditions. Closed boundaries are situated at the transition between land and water. Open boundaries are virtual "water-water" boundaries. These open boundaries have been introduced in order to limit the computational area.

At the closed boundaries the flow condition prohibiting flow through the boundary reads

$$\underline{n}\cdot\left.\begin{pmatrix}u\\v\end{pmatrix}\right|_{(x,y)=(x_b,y_b)} = 0 \quad \forall\sigma\in[-1,0]$$

where (x_b, y_b) is any point on the closed boundary and $\underline{n}$ consists of the first two components of the outward normal of the vertical boundary plane in that point. The slip condition imposed along the closed boundaries depend on the scale of the problem. In large scale problems the tangential shear stresses along closed boundaries can be neglected (free slip condition). For small scale problems this influence is not negligible and is taken into account through a partial slip condition.

At open boundaries the water level, the velocity or the discharge should be prescribed. The velocity at an open boundary is chosen perpendicular to that boundary for computational reasons. For an open boundary one of the following three boundary conditions can be prescribed. They are

$$\begin{aligned}\zeta &= F_\zeta(t) \quad \text{(prescribing the water level)},\\ U &= F_U(t) \quad \text{(prescribing the normal velocity component)},\\ Q &= F_Q(t) \quad \text{(prescribing the discharge)},\end{aligned} \tag{25}$$

where ζ is the free surface level (see page 5), U the depth-averaged normal velocity component (see page 7) and Q the discharge through the boundary plane. For simplicity we have assumed that the open boundary is perpendicular to the x-axis, so we only have to specify the velocity component along the x-axis. We will speak of a left and a right open boundary.

For the boundary conditions of the velocity and the discharge type a profile has to be prescribed in the vertical direction. This profile can be uniform or logarithmic. Also a complete 3D-profile can be prescribed in which for various depths different conditions are specified.

If an outgoing wave at an open boundary is not prescribed exactly then that wave will (partially) reflect at the boundary and propagate as a disturbance in the area. The boundary conditions in (25) will in general cause wave reflections. A non-reflective boundary condition is based on the Riemann invariants $U \pm 2\sqrt{gH}$. The boundary condition specified by the user would then be

$$U \pm 2\sqrt{gH} = F_R(t)$$

with "+" for the left and "−" for the right boundary. For numerical purposes it is convenient to have a linearised boundary condition.

Assumption 5. *The variations of the water level ζ (with respect to the reference plane) are small in comparison with the water depth d.*

Under this assumption the linearised Riemann invariants read

$$\begin{aligned} U \pm 2\sqrt{gH} = U \pm 2\sqrt{g(\zeta+d)} &= U \pm 2\sqrt{gd} \pm \zeta \frac{2g}{2\sqrt{g(\zeta+d)}} + \mathcal{O}(\zeta^2) \\ &\approx U \pm 2\sqrt{gd} \pm \zeta\sqrt{\frac{g}{d}}. \end{aligned}$$

To reduce the reflective properties of the water level and velocity boundary conditions in (25) the time-derivative of the Riemann invariant is added. The new boundary conditions are

$$\begin{aligned} \zeta + \alpha_\zeta \frac{\partial}{\partial t}\left(U \pm 2\sqrt{gH}\right) &= F_\zeta(t), \\ U + \alpha_U \frac{\partial}{\partial t}\left(U \pm 2\sqrt{gH}\right) &= F_U(t) \end{aligned}$$

for the water level and the velocity respectively. The reflection coefficients α_ζ and α_U should be chosen sufficiently small to damp short waves introduced by the initial conditions.

2.5 Turbulence closure models

In water flows small eddies occur due to turbulence. The grid used in numerical applications is usually too coarse to resolve the turbulent quantities u', v' and w'. Though initially they appear in the Reynolds-averaged Navier-Stokes equations (3), due to Assumption 2, the eddy viscosity concept (on page 5) they have vanished. However, an unknown parameter ν_t, the eddy viscosity, has been introduced, for which in shallow waters a horizontal and a vertical one are distinguished. In this section possible expressions or models for ν_t are treated, which are an important part of the eddy viscosity concept.

The horizontal eddy viscosity, ν_t^H, is usually chosen constant. Physically this is unsound, because the eddy viscosity is a flow property, but for large scale problems it has proved to be sufficiently accurate. The vertical eddy viscosity, ν_t^V, is computed according to one of the turbulence closure models. The models in which suitable expressions for ν_t are given or calculated are called turbulence closure models. The following models are available:

1. Constant coefficient.
2. Algebraic turbulence closure model.
3. k–L turbulence closure model.
4. k–ϵ turbulence closure model.

The first model is the simplest but also the most unrealistic as it will lead to a laminar flow. The other models are based on the eddy viscosity concept of Kolmogorov and Prandtl. In this concept the eddy viscosity is related to a characteristic length scale, $\mathcal{L}$, and a characteristic velocity scale, $\mathcal{U}$. This relation reads

$$\nu_t^V \sim \mathcal{L}\mathcal{U}.$$

The explicit form, also known as the Kolmogorov-Prandtl expression, is

$$\nu_t^V = c'_\mu l_m \sqrt{k},$$

where c'_μ is constant derived from the empirical constant c_μ in the k–ϵ model, l_m is the mixing length and k is the turbulent kinetic energy. The last three models differ in their prescription for l_m and k.

In the algebraic model an expression is given for l_m and k. For the mixing length one of the most common choices is given by the Bakhmetev distribution which reads

$$l_m = \kappa(z+d)\sqrt{1-\frac{z+d}{H}}$$

with κ the Von Kármán constant, $\kappa \approx 0.41$. An algebraic expression for k depends on the friction velocities or the velocity gradients.

In the k–L closure model the mixing length is analytically prescribed by $l_m = c_D k^{3/2}/\epsilon$, where c_D is a model coefficient, ϵ is the dissipation rate of turbulent kinetic energy and the turbulent kinetic energy follows from a transport equation.

The k–ϵ closure model uses transport equations for both the turbulent kinetic energy k as well as the dissipation rate of turbulent kinetic energy ϵ. These transport equations read

$$\frac{\partial k}{\partial t} + u\frac{\partial k}{\partial x} + v\frac{\partial k}{\partial y} + \frac{\omega}{H}\frac{\partial k}{\partial \sigma} = \frac{1}{H^2}\frac{\partial}{\partial \sigma}\left(\frac{\nu_t^V}{\sigma_k}\frac{\partial k}{\partial \sigma}\right) + P_k + B_k - \epsilon,$$
$$\frac{\partial \epsilon}{\partial t} + u\frac{\partial \epsilon}{\partial x} + v\frac{\partial \epsilon}{\partial y} + \frac{\omega}{H}\frac{\partial \epsilon}{\partial \sigma} = \frac{1}{H^2}\frac{\partial}{\partial \sigma}\left(\frac{\nu_t^V}{\sigma_\epsilon}\frac{\partial \epsilon}{\partial \sigma}\right) + P_\epsilon + B_\epsilon - c_{2\epsilon}\frac{\epsilon^2}{k},$$

where $c_{2\epsilon}$ is a model coefficient, $\sigma_{k/\epsilon}$ is the Prandtl-Schmidt number, $P_{k/\epsilon}$ is the production term and $B_{k/\epsilon}$ is the buoyancy term. These equations can be solved with appropriate initial and boundary conditions. Detailed descriptions of these models are beyond the scope of this report. For more information we refer to Launder and Spalding (1972) and Rodi (1985).

Large eddy simulation

Large eddies occur mainly in rivers, harbours and estuaries. Especially in harbours they are unwanted, since they cause sediment precipitation, making it necessary to dredge regularly.

The closure models mentioned above recognise the difference between a horizontal and a vertical eddy viscosity. These models prescribe a constant value for the horizontal eddy viscosity, because that is sufficient for large scale problems. However, this approach is physically unsound because the eddy viscosity depends on the local flow characteristics, and it should therefore not be used if large eddies (at least larger than the grid size) play an important role.

The field of large eddy simulation is still highly in development. An 'easy' possibility is to design a new closure model for the horizontal eddy viscosity. Uittenbogaard *et al.* (1992) proposed the following definition for the horizontal eddy viscosity

$$\nu_t^H = \nu_t^{2D} + \nu_t^V,$$

where ν_t^{2D} is the part due to "2D turbulence" and ν_t^V, the vertical eddy viscosity, is the part due to "3D turbulence". Bijvelds (2001) constructed the 'two-length-scale k–ϵ model' to calculate ν_t^{2D} in which is assumed that large eddies are quasi-2D, so a depth-averaged version of the k–ϵ closure model can be used.

3 Numerical scheme for the shallow-water equations

The analytical solution of the shallow-water equations can only be calculated in a very small number of cases, which however do not occur in nature. A numerical approximation is therefore almost inevitable. In Delft3D-FLOW a finite difference scheme on a staggered grid is chosen using an ADI solver in conjunction with a Gauss-Seidel iteration. In the next sections these numerical methods will be discussed.

3.1 Shallow-water equations in appropriate form

The equations which are actually going to be numerically approximated are the horizontal momentum equations (18) and (19), the continuity equation (16) and the integrated continuity equation (17). The pressure in the momentum equations is given by equation (14). Substituting (14) in the pressure terms of the momentum equations in x- and y-direction, setting the density constant and neglecting the atmospheric pressure gradient, these terms reduce to the barotropic terms

$$-g\frac{\partial \zeta}{\partial x} \quad \text{and} \quad -g\frac{\partial \zeta}{\partial y},$$

respectively. For the horizontal eddy viscosity terms F_x and F_y we will use the simplified equations in (20).

For convenience we repeat the above mentioned equations, taking the remarks into account,

$$\frac{\partial u}{\partial t} + u\frac{\partial u}{\partial x} + v\frac{\partial u}{\partial y} + \frac{\omega}{H}\frac{\partial u}{\partial \sigma} = -g\frac{\partial \zeta}{\partial x} + fv + \nu_t^H\left(\frac{\partial^2 u}{\partial x^2} + \frac{\partial^2 u}{\partial y^2}\right) + \frac{1}{H^2}\frac{\partial}{\partial \sigma}\left(\nu_t^V\frac{\partial u}{\partial \sigma}\right), \tag{26a}$$

$$\frac{\partial v}{\partial t} + u\frac{\partial v}{\partial x} + v\frac{\partial v}{\partial y} + \frac{\omega}{H}\frac{\partial v}{\partial \sigma} = -g\frac{\partial \zeta}{\partial y} - fu + \nu_t^H\left(\frac{\partial^2 v}{\partial x^2} + \frac{\partial^2 v}{\partial y^2}\right) + \frac{1}{H^2}\frac{\partial}{\partial \sigma}\left(\nu_t^V\frac{\partial v}{\partial \sigma}\right), \tag{26b}$$

$$\frac{\partial \zeta}{\partial t} + \frac{\partial HU}{\partial x} + \frac{\partial HV}{\partial y} = 0, \tag{26c}$$

$$\frac{\partial \zeta}{\partial t} + \frac{\partial Hu}{\partial x} + \frac{\partial Hv}{\partial y} + \frac{\partial \omega}{\partial \sigma} = 0. \tag{26d}$$

3.2 Alternating Direction Implicit schemes in general

When working on a two-dimensional problem using implicit schemes, usually a large banded matrix equation has to be solved. An implicit numerical scheme for the two-dimensional heat equation,

$$\frac{\partial u}{\partial t} = \alpha\left(\frac{\partial^2 u}{\partial x^2} + \frac{\partial^2 u}{\partial y^2}\right), \tag{27}$$

for example, would look like

$$\frac{u_{m,n}^{p+1} - u_{m,n}^{p}}{\triangle t} = \alpha(\delta_x^2 u_{m,n}^{p+1} + \delta_y^2 u_{m,n}^{p+1})$$

with

$$\delta_x^2 u_{m,n}^{p+1} = (u_{m-1,n}^{p+1} - 2u_{m,n}^{p+1} + u_{m+1,n}^{p+1})/\triangle x^2 \quad \text{and}$$
$$\delta_y^2 u_{m,n}^{p+1} = (u_{m,n-1}^{p+1} - 2u_{m,n}^{p+1} + u_{m,n+1}^{p+1})/\triangle y^2.$$

Solving this equation by Gaussian elimination would be too expensive due to fill-in. The alternating direction implicit (ADI) schemes are a good alternative, because only tridiagonal

matrix equations have to be solved. The idea is to use implicit numerical approximations in one direction and explicit ones in the other direction.

We will discuss one of the most common ADI schemes, the Peaceman-Rachford scheme, for the two-dimensional heat equation. This ADI scheme uses a time step of $\triangle t/2$ and the direction in which implicit numerical approximations are used alternates. The scheme reads

$$\frac{u_{m,n}^{p+\frac{1}{2}} - u_{m,n}^{p}}{\triangle t/2} = \alpha\delta_x^2 u_{m,n}^{p+\frac{1}{2}} + \alpha\delta_y^2 u_{m,n}^{p} \tag{28a}$$

$$\frac{u_{m,n}^{p+1} - u_{m,n}^{p+\frac{1}{2}}}{\triangle t/2} = \alpha\delta_x^2 u_{m,n}^{p+\frac{1}{2}} + \alpha\delta_y^2 u_{m,n}^{p+1}. \tag{28b}$$

In equation (28a) the derivative with respect to x is evaluated implicitly and the derivative with respect to y explicitly and vice versa in equation (28b). Note that both matrix equations are tridiagonal. From now on we will refer to (28) as one iteration, divided in two stages.

Stability

For stability analysis we use a Von Neumann stability method. Let

$$u_{m,n}^{p} = G^p e^{i\theta_x m} e^{i\theta_y n},$$

where i is the imaginary unit, $\theta_x, \theta_y \in [0, 2\pi]$ and $G \in \mathbb{R}$, and substitute this expression in the first stage, equation (28a). After cancelling several factors this results in

$$G^{p+\frac{1}{2}} = G^p + \frac{1}{2} r_x G^{p+\frac{1}{2}}[e^{-i\theta_x \triangle x} - 2 + e^{i\theta_x \triangle x}] + \frac{1}{2} r_y G^p [e^{-i\theta_y \triangle y} - 2 + e^{i\theta_y \triangle y}]$$

with $r_x = \alpha\triangle t/\triangle x^2$ and $r_y = \alpha\triangle t/\triangle y^2$. Further manipulation leads to the following relation for the amplification factor G:

$$\sqrt{G} = \frac{1 + r_y[\cos\beta_y - 1]}{1 - r_x[\cos\beta_x - 1]} = \frac{1 - 2r_y \sin^2\frac{1}{2}\beta_y}{1 + 2r_x \sin^2\frac{1}{2}\beta_x}$$

with $\beta_x = \theta_x \triangle x$ and $\beta_y = \theta_y \triangle y$. For the second stage the relation for the amplification factor reads

$$\sqrt{G} = \frac{1 + r_x[\cos\beta_x - 1]}{1 - r_y[\cos\beta_y - 1]} = \frac{1 - 2r_x \sin^2\frac{1}{2}\beta_x}{1 + 2r_y \sin^2\frac{1}{2}\beta_y}.$$

Thus the amplification factor for the whole time step $\triangle t$ is

$$G = \frac{(1 - 2r_x \sin^2\frac{1}{2}\beta_x)(1 - 2r_y \sin^2\frac{1}{2}\beta_y)}{(1 + 2r_x \sin^2\frac{1}{2}\beta_x)(1 + 2r_y \sin^2\frac{1}{2}\beta_y)}.$$

Since r_x and r_y are both positive and the sine terms are at most equal to one, the amplification factor is always smaller than one. Hence this ADI scheme is unconditionally stable. Note that each stage separately is conditionally stable with the conditions $r_y \leq 1$ and $r_x \leq 1$, respectively.

Consistency

Next we will discuss the consistency (accuracy) of the scheme. Therefore we rewrite the equations (28a) and (28b) as

$$(1 - \tfrac{1}{2}\triangle t\,\alpha\,\delta_x^2) u_{m,n}^{p+\frac{1}{2}} = (1 + \tfrac{1}{2}\triangle t\,\alpha\,\delta_y^2) u_{m,n}^{p} \tag{29a}$$

$$(1 - \tfrac{1}{2}\triangle t\,\alpha\,\delta_y^2) u_{m,n}^{p+1} = (1 + \tfrac{1}{2}\triangle t\,\alpha\,\delta_x^2) u_{m,n}^{p+\frac{1}{2}}. \tag{29b}$$

After multiplication of (29a) with $(1 + \frac{1}{2}\triangle t\,\alpha\,\delta_x^2)$ the operators on the left-hand side are commutable. Having done so we substitute (29b) in it, resulting in

$$(1 - \tfrac{1}{2}\triangle t\,\alpha\,\delta_x^2)(1 - \tfrac{1}{2}\triangle t\,\alpha\,\delta_y^2)u_{m,n}^{p+1} = (1 + \tfrac{1}{2}\triangle t\,\alpha\,\delta_x^2)(1 + \tfrac{1}{2}\triangle t\,\alpha\,\delta_y^2)u_{m,n}^{p} \tag{30}$$

Expanding the terms in equation (30) the ADI scheme is equivalent to

$$\begin{aligned}\frac{u_{m,n}^{p+1} - u_{m,n}^{p}}{\triangle t} =& \frac{\alpha}{2}\frac{\delta_x^2}{\triangle x^2}(u_{m,n}^{p+1} + u_{m,n}^{p}) + \frac{\alpha}{2}\frac{\delta_y^2}{\triangle y^2}(u_{m,n}^{p+1} + u_{m,n}^{p}) \\ & - \frac{\alpha\triangle t}{4}\frac{\delta_x^2}{\triangle x^2}\frac{\delta_y^2}{\triangle y^2}(u_{m,n}^{p+1} - u_{m,n}^{p})\end{aligned} \tag{31}$$

Using Taylor series expansion on equation (31), we see that

$$\begin{aligned}&\left[\frac{\partial u}{\partial t}\right]_{m,n}^{p} + \frac{1}{2}\triangle t\left[\frac{\partial^2 u}{\partial t^2}\right]_{m,n}^{p} + \mathcal{O}(\triangle t^2) = \\ &\qquad \alpha\left[\frac{\partial^2 u}{\partial x^2}\right]_{m,n}^{p} + \tfrac{1}{2}\alpha\triangle t\left[\frac{\partial^3 u}{\partial x^2\partial t}\right]_{m,n}^{p} + \mathcal{O}(\triangle x^2) + \mathcal{O}(\triangle t\triangle x^2) \\ &\quad + \alpha\left[\frac{\partial^2 v}{\partial x^2}\right]_{m,n}^{p} + \tfrac{1}{2}\alpha\triangle t\left[\frac{\partial^3 v}{\partial y^2\partial t}\right]_{m,n}^{p} + \mathcal{O}(\triangle y^2) + \mathcal{O}(\triangle t\triangle y^2) \\ &\quad - \tfrac{1}{4}\alpha\triangle t^2\left[\frac{\partial u}{\partial x^2\partial y^2\partial t}\right]_{m,n}^{p} + \mathcal{O}(\triangle t^2\triangle x^2) + \mathcal{O}(\triangle t^2\triangle y^2) + \mathcal{O}(\triangle t^3)\end{aligned} \tag{32}$$

Using equation (27) on (32) (twice!) shows that the Peaceman-Rachford scheme is second order accurate in $\triangle t$, $\triangle x$ and $\triangle y$. For more details on ADI schemes and the Peaceman-Rachford scheme in particular we refer to Mitchell and Griffiths (1980).

3.3 Grid and numerical scheme

This section is largely taken from Stelling (1984). More information on discretisations on staggered grids can be found in Wesseling (2000).

The horizontal grid is the so-called Arakawa C grid, a staggered grid. This means that the variables are arranged on the grid in a special way. The different variables are not calculated at the same physical points in the horizontal plane. Figure 2 shows an example of a staggered grid.

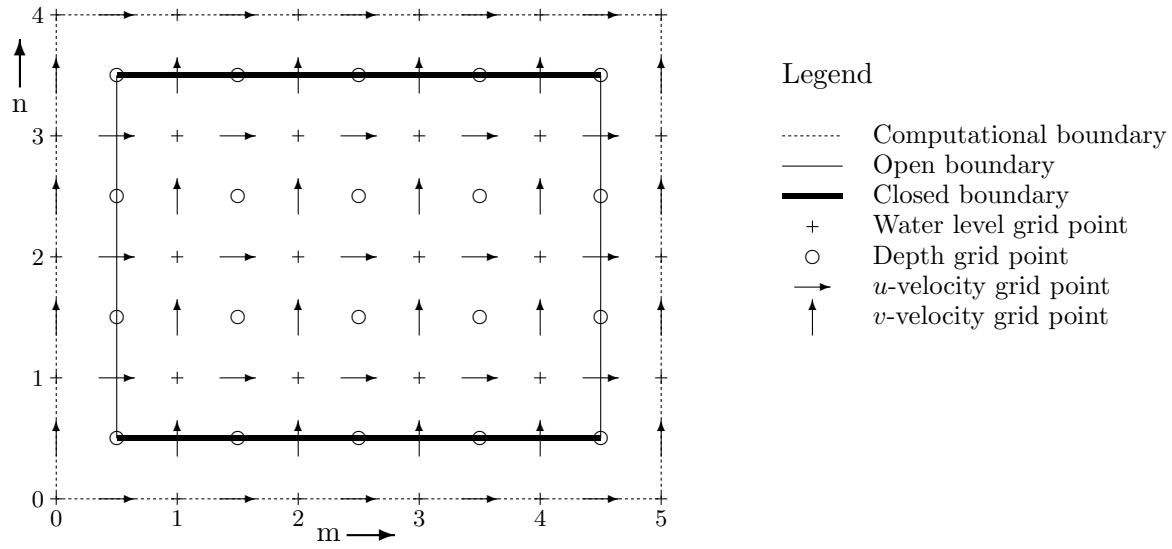

Figure 2. The horizontal staggered grid.

In general we will refer to the horizontal grid indices with m and n for the x- and y-direction, respectively; and with M and N for their maximums.

The open and closed boundaries in Figure 2 form the model boundary. Only points within this boundary are calculated. For the open boundaries either the normal velocity component at the boundary (e.g. at grid coordinates $(\frac{1}{2}, 2)$) or the water level just outside the boundary (e.g. at $(0, 2)$) should be prescribed.

In the vertical direction we define a number of layers, so-called σ-layers. The number of layers is K. We will use index k to refer to the k^{th} layer with $k = 1$ for the surface layer and $k = K$ for the bottom layer. The discretisation in σ-direction is not necessarily equidistant, so the various layers may differ with respect to their thickness, $\Delta\sigma_k$. Also in the vertical direction a staggered grid is used. Figure 3 shows a single vertical grid cell for an arbitrary value of n.

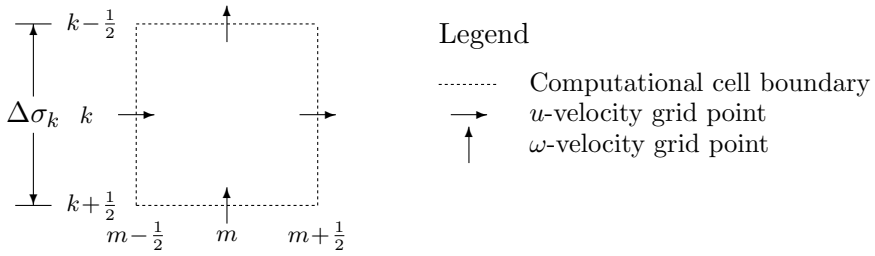

Figure 3. A cell from the vertical staggered grid.

The numerical approximations will be given for both stages and if necessary due to the staggered grid averaged quantities are introduced. At the inner points of the grid each term of the equations (26a-d) is approximated as follows:

1. Discretisation of $\dfrac{\partial u}{\partial t}$ at $(m+\frac{1}{2}, n, k)$

   stage 1: $(u^{p+\frac{1}{2}} - u^p)/\frac{1}{2}\tau$

   stage 2: $(u^{p+1} - u^{p+\frac{1}{2}})/\frac{1}{2}\tau$

2. Discretisation of $\dfrac{\partial v}{\partial t}$ at $(m, n+\frac{1}{2}, k)$ is equivalent to the discretisation of $\dfrac{\partial u}{\partial t}$.

3. Discretisation of $\dfrac{\partial \zeta}{\partial t}$ at (m, n) is equivalent to the discretisation of $\dfrac{\partial u}{\partial t}$.

4. Horizontal advection term $u\dfrac{\partial u}{\partial x}$ at $(m+\frac{1}{2}, n, k)$

   stage 1: $u^{p+\frac{1}{2}}_{m+\frac{1}{2},n}(u^p_{m+1\frac{1}{2},n} - u^p_{m-\frac{1}{2},n})/2\triangle x$

   stage 2: $\begin{cases} u^{p+\frac{1}{2}}_{m+\frac{1}{2},n}(3u^{p+1}_{m+\frac{1}{2},n} - 4u^{p+1}_{m-\frac{1}{2},n} + u^{p+1}_{m-1\frac{1}{2},n})/2\triangle x, & \text{if} \quad u^{p+\frac{1}{2}}_{m+\frac{1}{2},n} > 0 \\ u^{p+\frac{1}{2}}_{m+\frac{1}{2},n}(-3u^{p+1}_{m+\frac{1}{2},n} + 4u^{p+1}_{m+1\frac{1}{2},n} - u^{p+1}_{m+2\frac{1}{2},n})/2\triangle x, & \text{if} \quad u^{p+\frac{1}{2}}_{m+\frac{1}{2},n} \leq 0 \end{cases}$

   In the first stage the derivative is treated in an explicit way and approximated with a central difference scheme; in the second stage it is approximated with an implicit upwind scheme.

5. Horizontal advection term $v\dfrac{\partial v}{\partial y}$ at $(m, n+\frac{1}{2}, k)$

stage 1: $\begin{cases} v^p_{m,n+\frac{1}{2}}(3v^{p+\frac{1}{2}}_{m,n+\frac{1}{2}} - 4v^{p+\frac{1}{2}}_{m,n-\frac{1}{2}} + v^{p+\frac{1}{2}}_{m,n-1\frac{1}{2}})/2\triangle y, & \text{if} \quad v^p_{m,n+\frac{1}{2}} > 0 \\ v^p_{m,n+\frac{1}{2}}(-3v^{p+\frac{1}{2}}_{m,n+\frac{1}{2}} + 4v^{p+\frac{1}{2}}_{m,n+1\frac{1}{2}} - v^{p+\frac{1}{2}}_{m,n+2\frac{1}{2}})/2\triangle y, & \text{if} \quad v^p_{m,n+\frac{1}{2}} \le 0 \end{cases}$

stage 2: $v^{p+1}_{m,n+\frac{1}{2}}(v^{p+\frac{1}{2}}_{m,n+1\frac{1}{2}} - v^{p+\frac{1}{2}}_{m,n-\frac{1}{2}})/2\triangle y$

In the first stage the derivative is approximated with an implicit upwind scheme; in the second stage it is treated in an explicit way and approximated with a central difference scheme.

6. Horizontal advection term $v\dfrac{\partial u}{\partial y}$ at $(m+\frac{1}{2}, n, k)$

stage 1: $\bar{v}^{p+\frac{1}{2}}_{m+\frac{1}{2},n}(u^p_{m+\frac{1}{2},n+1} - u^p_{m+\frac{1}{2},n-1})/2\triangle y$

stage 2: $\begin{cases} \bar{v}^{p+\frac{1}{2}}_{m+\frac{1}{2},n}(3u^{p+1}_{m+\frac{1}{2},n} - 4u^{p+1}_{m+\frac{1}{2},n-1} + u^{p+1}_{m+\frac{1}{2},n-2})/2\triangle y, & \text{if} \quad \bar{v}^{p+\frac{1}{2}}_{m+\frac{1}{2},n} > 0 \\ \bar{v}^{p+\frac{1}{2}}_{m+\frac{1}{2},n}(-3u^{p+1}_{m+\frac{1}{2},n} + 4u^{p+1}_{m+\frac{1}{2},n+1} - u^{p+1}_{m+\frac{1}{2},n+2})/2\triangle y, & \text{if} \quad \bar{v}^{p+\frac{1}{2}}_{m+\frac{1}{2},n} \le 0 \end{cases}$

where $\bar{v}^{p+\frac{1}{2}}_{m+\frac{1}{2},n} = \frac{1}{4}(v^{p+\frac{1}{2}}_{m,n+\frac{1}{2}} + v^{p+\frac{1}{2}}_{m+1,n+\frac{1}{2}} + v^{p+\frac{1}{2}}_{m,n-\frac{1}{2}} + v^{p+\frac{1}{2}}_{m+1,n-\frac{1}{2}})$, the averaged value for $v^{p+\frac{1}{2}}$ at $(m+\frac{1}{2}, n, k)$.

7. Horizontal advection term $u\dfrac{\partial v}{\partial x}$ at $(m, n+\frac{1}{2}, k)$

stage 1: $\begin{cases} \bar{u}^p_{m,n+\frac{1}{2}}(3v^{p+\frac{1}{2}}_{m,n+\frac{1}{2}} - 4v^{p+\frac{1}{2}}_{m-1,n+\frac{1}{2}} + v^{p+\frac{1}{2}}_{m-2,n+\frac{1}{2}})/2\triangle x, & \text{if} \quad \bar{u}^p_{m,n+\frac{1}{2}} > 0 \\ \bar{u}^p_{m,n+\frac{1}{2}}(-3v^{p+\frac{1}{2}}_{m,n+\frac{1}{2}} + 4v^{p+\frac{1}{2}}_{m+1,n+\frac{1}{2}} - v^{p+\frac{1}{2}}_{m+2,n+\frac{1}{2}})/2\triangle x, & \text{if} \quad \bar{u}^p_{m,n+\frac{1}{2}} \le 0 \end{cases}$

stage 2: $\bar{u}^{p+1}_{m,n+\frac{1}{2}}(v^{p+\frac{1}{2}}_{m+1,n+\frac{1}{2}} - v^{p+\frac{1}{2}}_{m-1,n+\frac{1}{2}})/2\triangle x$

where $\bar{u}^p_{m,n+\frac{1}{2}} = \frac{1}{4}(u^p_{m+\frac{1}{2},n} + u^p_{m+\frac{1}{2},n+1} + u^p_{m-\frac{1}{2},n} + u^p_{m-\frac{1}{2},n+1})$, the averaged value for u^p at $(m, n+\frac{1}{2}, k)$.

8. Vertical advection term $\dfrac{\omega}{H}\dfrac{\partial u}{\partial \sigma}$ at $(m+\frac{1}{2}, n, k)$

stage 1: $\dfrac{\bar{\omega}^p_k}{\frac{1}{2}h^p_{k-1}+h^p_k+\frac{1}{2}h^p_{k+1}}\left[\dfrac{h^p_k+h^p_{k+1}}{h^p_{k-1}+h^p_k}\left(u^{p+\frac{1}{2}}_{k-1} - u^{p+\frac{1}{2}}_k\right) + \dfrac{h^p_{k-1}+h^p_k}{h^p_k+h^p_{k+1}}\left(u^{p+\frac{1}{2}}_k - u^{p+\frac{1}{2}}_{k+1}\right)\right]$

stage 2: $\dfrac{\bar{\omega}^{p+\frac{1}{2}}_k}{\frac{1}{2}h^{p+\frac{1}{2}}_{k-1}+h^{p+\frac{1}{2}}_k+\frac{1}{2}h^{p+\frac{1}{2}}_{k+1}}\left[\dfrac{h^{p+\frac{1}{2}}_k+h^{p+\frac{1}{2}}_{k+1}}{h^{p+\frac{1}{2}}_{k-1}+h^{p+\frac{1}{2}}_k}\left(u^{p+1}_{k-1} - u^{p+1}_k\right) + \dfrac{h^{p+\frac{1}{2}}_{k-1}+h^{p+\frac{1}{2}}_k}{h^{p+\frac{1}{2}}_k+h^{p+\frac{1}{2}}_{k+1}}\left(u^{p+1}_k - u^{p+1}_{k+1}\right)\right]$

where

$$\bar{\omega}^p_k = \bar{\omega}^p_{m+\frac{1}{2},n,k} = \tfrac{1}{4}(\omega^p_{m,n,k-\frac{1}{2}} + \omega^p_{m,n,k+\frac{1}{2}} + \omega^p_{m+1,n,k-\frac{1}{2}} + \omega^p_{m+1,n,k+\frac{1}{2}}),$$

the averaged value of ω^p at $(m+\frac{1}{2}, n, k)$, and $h^p_{m+\frac{1}{2},n,k}$ is defined as $\Delta\sigma_k \bar{H}^p_{m+\frac{1}{2},n}$ with

$$\bar{H}^p_{m+\frac{1}{2},n} = \tfrac{1}{2}(\zeta^p_{m,n} + \zeta^p_{m+1,n} + d_{m+\frac{1}{2},n-\frac{1}{2}} + d_{m+\frac{1}{2},n+\frac{1}{2}}),$$

the averaged value of H^p at $(m+\frac{1}{2}, n)$.

9. Vertical advection term $\dfrac{\omega}{H}\dfrac{\partial v}{\partial \sigma}$ at $(m, n+\frac{1}{2}, k)$

   stage 1: $\dfrac{\bar{\omega}_k^p}{\frac{1}{2}h_{k-1}^p+h_k^p+\frac{1}{2}h_{k+1}^p}\left[\dfrac{h_k^p+h_{k+1}^p}{h_{k-1}^p+h_k^p}\left(v_{k-1}^{p+\frac{1}{2}}-v_k^{p+\frac{1}{2}}\right)+\dfrac{h_{k-1}^p+h_k^p}{h_k^p+h_{k+1}^p}\left(v_k^{p+\frac{1}{2}}-v_{k+1}^{p+\frac{1}{2}}\right)\right]$

   stage 2: $\dfrac{\bar{\omega}_k^{p+\frac{1}{2}}}{\frac{1}{2}h_{k-1}^{p+\frac{1}{2}}+h_k^{p+\frac{1}{2}}+\frac{1}{2}h_{k+1}^{p+\frac{1}{2}}}\left[\dfrac{h_k^{p+\frac{1}{2}}+h_{k+1}^{p+\frac{1}{2}}}{h_{k-1}^{p+\frac{1}{2}}+h_k^{p+\frac{1}{2}}}\left(v_{k-1}^{p+1}-v_k^{p+1}\right)+\dfrac{h_{k-1}^{p+\frac{1}{2}}+h_k^{p+\frac{1}{2}}}{h_k^{p+\frac{1}{2}}+h_{k+1}^{p+\frac{1}{2}}}\left(v_k^{p+1}-v_{k+1}^{p+1}\right)\right]$

10. Barotropic term $-g\dfrac{\partial \zeta}{\partial x}$ at $(m+\frac{1}{2}, n, k)$

    stage 1: $-g\left(\zeta_{m+1,n}^{p+\frac{1}{2}}-\zeta_{m,n}^{p+\frac{1}{2}}\right)/\triangle x$

    stage 2: the same expression as in the first stage.

    Note that in the first stage the expression is implicit and it is explicit in the second stage.

11. Barotropic term $-g\dfrac{\partial \zeta}{\partial y}$ at $(m, n+\frac{1}{2}, k)$

    stage 1: $-g\left(\zeta_{m,n+1}^{p}-\zeta_{m,n}^{p}\right)/\triangle y$

    stage 2: $-g\left(\zeta_{m,n+1}^{p+1}-\zeta_{m,n}^{p+1}\right)/\triangle y$

    Note that in the first stage the expression is explicit and it is implicit in the second stage.

12. Horizontal viscosity term $\nu_t^H\left(\dfrac{\partial^2 u}{\partial x^2}+\dfrac{\partial^2 u}{\partial y^2}\right)$ at $(m+\frac{1}{2}, n, k)$

    stage 1: 0

    stage 2: $2\nu_t^H\left[S_{xx}(u_{m+\frac{1}{2},n}^{p+1})+S_{yy}(u_{m+\frac{1}{2},n}^{p+1})\right]$

    with

$$S_{xx}(u_{m+\frac{1}{2},n}^{p+1}) = (u_{m-\frac{1}{2},n}^{p+1}-2u_{m+\frac{1}{2},n}^{p+1}+u_{m+1\frac{1}{2},n}^{p+1})/\triangle x^2,$$
$$S_{yy}(u_{m+\frac{1}{2},n}^{p+1}) = (u_{m+\frac{1}{2},n-1}^{p+1}-2u_{m+\frac{1}{2},n}^{p+1}+u_{m+\frac{1}{2},n+1}^{p+1})/\triangle y^2.$$

    In the first stage this term is neglected, while in the second stage it is computed for the whole time step (thus twice as large).

13. Horizontal viscosity term $\nu_t^H\left(\dfrac{\partial^2 v}{\partial x^2}+\dfrac{\partial^2 v}{\partial y^2}\right)$ at $(m, n+\frac{1}{2}, k)$

    stage 1: $2\nu_t^H\left[S_{xx}(v_{m,n+\frac{1}{2}}^{p+\frac{1}{2}})+S_{yy}(v_{m,n+\frac{1}{2}}^{p+\frac{1}{2}})\right]$

    stage 2: 0

14. Vertical viscosity term $\dfrac{1}{H^2}\dfrac{\partial}{\partial \sigma}\left(\nu_t^V\dfrac{\partial u}{\partial \sigma}\right)$ at $(m+\frac{1}{2}, n, k)$

    stage 1: $\dfrac{1}{h_k^p}\left[\nu_{k-\frac{1}{2}}^V\dfrac{u_{k-1}^{p+\frac{1}{2}}-u_k^{p+\frac{1}{2}}}{\frac{1}{2}\left(h_{k-1}^p+h_k^p\right)}-\nu_{k+\frac{1}{2}}^V\dfrac{u_k^{p+\frac{1}{2}}-u_{k+1}^{p+\frac{1}{2}}}{\frac{1}{2}\left(h_k^p+h_{k+1}^p\right)}\right]$

    stage 2: $\dfrac{1}{h_k^{p+\frac{1}{2}}}\left[\nu_{k-\frac{1}{2}}^V\dfrac{u_{k-1}^{p+1}-u_k^{p+1}}{\frac{1}{2}\left(h_{k-1}^{p+\frac{1}{2}}+h_k^{p+\frac{1}{2}}\right)}-\nu_{k+\frac{1}{2}}^V\dfrac{u_k^{p+1}-u_{k+1}^{p+1}}{\frac{1}{2}\left(h_k^{p+\frac{1}{2}}+h_{k+1}^{p+\frac{1}{2}}\right)}\right]$

The vertical eddy viscosity ν_t^V is calculated or determined through one of the turbulence closure models. This is done in an explicit way. In both stages only the flow velocity component is taken implicitly.

15. Vertical viscosity term $\frac{1}{H^2}\frac{\partial}{\partial\sigma}\left(\nu_t^V\frac{\partial v}{\partial\sigma}\right)$ at $(m,n+\frac{1}{2},k)$ is discretised in a similar manner as $\frac{1}{H^2}\frac{\partial}{\partial\sigma}\left(\nu_t^V\frac{\partial u}{\partial\sigma}\right)$.

16. Coriolis term fv at $(m+\frac{1}{2},n,k)$

    stage 1: $f\bar{v}^{p+\frac{1}{2}}_{m+\frac{1}{2},n}$

    stage 2: the same expression as in the first stage.

    Note that in the first stage the expression is implicit and it is explicit in the second stage.

17. Coriolis term $-fu$ at $(m,n+\frac{1}{2},k)$

    stage 1: $-f\bar{u}^{p}_{m,n+\frac{1}{2}}$

    stage 2: $-f\bar{u}^{p+1}_{m,n+\frac{1}{2}}$

    Note that in the first stage the expression is explicit and it is implicit in the second stage.

18. $\frac{\partial HU}{\partial x}$ at (m,n)

    stage 1: $\sum_k\Delta\sigma_k\left(\bar{H}^{p+\frac{1}{2}}_{m+\frac{1}{2},n,k}u^{p+\frac{1}{2}}_{m+\frac{1}{2},n,k}-\bar{H}^{p+\frac{1}{2}}_{m-\frac{1}{2},n,k}u^{p+\frac{1}{2}}_{m-\frac{1}{2},n,k}\right)/\triangle x$

    stage 2: the same expression as in the first stage.

    Note that in the first stage the expression is implicit and it is explicit in the second stage.

19. $\frac{\partial HV}{\partial y}$ at (m,n)

    stage 1: $\sum_k\Delta\sigma_k\left(\bar{H}^{p}_{m,n+\frac{1}{2},k}v^{p}_{m,n+\frac{1}{2},k}-\bar{H}^{p}_{m,n-\frac{1}{2},k}v^{p}_{m,n-\frac{1}{2},k}\right)/\triangle y$

    stage 2: $\sum_k\Delta\sigma_k\left(\bar{H}^{p+1}_{m,n+\frac{1}{2},k}v^{p+1}_{m,n+\frac{1}{2},k}-\bar{H}^{p+1}_{m,n-\frac{1}{2},k}v^{p+1}_{m,n-\frac{1}{2},k}\right)/\triangle y$

20. $\frac{\partial Hu}{\partial x}$ at (m,n,k)

    stage 1: $\left(\bar{H}^{p+\frac{1}{2}}_{m+\frac{1}{2},n,k}u^{p+\frac{1}{2}}_{m+\frac{1}{2},n,k}-\bar{H}^{p+\frac{1}{2}}_{m-\frac{1}{2},n,k}u^{p+\frac{1}{2}}_{m-\frac{1}{2},n,k}\right)/\triangle x$

    stage 2: the same expression as in the first stage.

    Note that in the first stage the expression is implicit and it is explicit in the second stage.

21. $\frac{\partial Hv}{\partial y}$ at (m,n,k)

    stage 1: $\left(\bar{H}^{p}_{m,n+\frac{1}{2},k}v^{p}_{m,n+\frac{1}{2},k}-\bar{H}^{p}_{m,n-\frac{1}{2},k}v^{p}_{m,n-\frac{1}{2},k}\right)/\triangle y$

    stage 2: $\left(\bar{H}^{p+1}_{m,n+\frac{1}{2},k}v^{p+1}_{m,n+\frac{1}{2},k}-\bar{H}^{p+1}_{m,n-\frac{1}{2},k}v^{p+1}_{m,n-\frac{1}{2},k}\right)/\triangle y$

22. $\dfrac{\partial \omega}{\partial \sigma}$ at (m,n,k)

stage 1: $\left(\omega_{k-\frac{1}{2}}^{p+\frac{1}{2}} - \omega_{k+\frac{1}{2}}^{p+\frac{1}{2}}\right)/\Delta\sigma_k$

stage 2: $\left(\omega_{k-\frac{1}{2}}^{p+1} - \omega_{k+\frac{1}{2}}^{p+1}\right)/\Delta\sigma_k$

For clarity we will give the equations (26a-d) in approximated discrete form using symbols to represent derivatives. Then the first stage reads

$$\begin{aligned}\frac{u^{p+\frac{1}{2}} - u^p}{\tau/2} + u^{p+\frac{1}{2}}\, S_x(u^p) + v^{p+\frac{1}{2}}\, S_y(u^p) + \omega^p\, S_\sigma(u^{p+\frac{1}{2}}) \\ = -g\, S_x(\zeta^{p+\frac{1}{2}}) + S_{\sigma\sigma}(u^{p+\frac{1}{2}}) + f v^{p+\frac{1}{2}},\end{aligned} \tag{33a}$$

$$\begin{aligned}\frac{v^{p+\frac{1}{2}} - v^p}{\tau/2} + u^p\, S_{1x}(v^{p+\frac{1}{2}}) + v^p\, S_{1y}(v^{p+\frac{1}{2}}) + \omega^p\, S_\sigma(v^{p+\frac{1}{2}}) \\ = -g\, S_y(\zeta^p) + 2\nu_t^H[S_{xx}(v^{p+\frac{1}{2}}) + S_{yy}(v^{p+\frac{1}{2}})] + S_{\sigma\sigma}(v^{p+\frac{1}{2}}) - f u^p,\end{aligned} \tag{33b}$$

$$\frac{\zeta^{p+\frac{1}{2}} - \zeta^p}{\tau/2} + S_x\left(H^{p+\frac{1}{2}} \sum_k \Delta\sigma_k u_k^{p+\frac{1}{2}}\right) + S_y\left(H^p \sum_k \Delta\sigma_k v_k^p\right) = 0, \tag{33c}$$

$$\frac{\omega_{k-\frac{1}{2}}^{p+\frac{1}{2}} - \omega_{k+\frac{1}{2}}^{p+\frac{1}{2}}}{\Delta\sigma_k} + \frac{\zeta^{p+\frac{1}{2}} - \zeta^p}{\tau/2} + S_x(H^{p+\frac{1}{2}} u_k^{p+\frac{1}{2}}) + S_y(H^p v_k^p) = 0. \tag{33d}$$

The symbols S_x and S_y represent second order accurate central difference schemes of the first derivatives with respect to respectively x and y. The second order accurate upwind schemes for the first derivatives are represented by S_{1x} and S_{1y}. The symbols S_{xx} and S_{yy} are defined at item 12. in the list of approximated terms. And the symbols S_σ and $S_{\sigma\sigma}$ represent the discretisations in items 8. (and 9.) and 14. respectively.

The second stage reads

$$\begin{aligned}\frac{u^{p+1} - u^{p+\frac{1}{2}}}{\tau/2} + u^{p+\frac{1}{2}}\, S_{1x}(u^{p+1}) + v^{p+\frac{1}{2}}\, S_{1y}(u^{p+1}) + \omega^{p+\frac{1}{2}}\, S_\sigma(u^{p+1}) \\ = -g\, S_x(\zeta^{p+\frac{1}{2}}) + 2\nu_t^H[S_{xx}(u^{p+1}) + S_{yy}(u^{p+1})] + S_{\sigma\sigma}(u^{p+1}) + f v^{p+\frac{1}{2}},\end{aligned} \tag{34a}$$

$$\begin{aligned}\frac{v^{p+1} - v^{p+\frac{1}{2}}}{\tau/2} + u^{p+1}\, S_x(v^{p+\frac{1}{2}}) + v^{p+1}\, S_y(v^{p+\frac{1}{2}}) + \omega^{p+\frac{1}{2}}\, S_\sigma(v^{p+1}) \\ = -g\, S_y(\zeta^{p+1}) + S_{\sigma\sigma}(v^{p+1}) - f u^{p+1},\end{aligned} \tag{34b}$$

$$\frac{\zeta^{p+1} - \zeta^{p+\frac{1}{2}}}{\tau/2} + S_x\left(H^{p+\frac{1}{2}} \sum_k \Delta\sigma_k u_k^{p+\frac{1}{2}}\right) + S_y\left(H^{p+1} \sum_k \Delta\sigma_k v_k^{p+1}\right) = 0, \tag{34c}$$

$$\frac{\omega_{k-\frac{1}{2}}^{p+1} - \omega_{k+\frac{1}{2}}^{p+1}}{\Delta\sigma_k} + \frac{\zeta^{p+1} - \zeta^{p+\frac{1}{2}}}{\tau/2} + S_x(H^{p+\frac{1}{2}} u_k^{p+\frac{1}{2}}) + S_y(H^{p+1} v_k^{p+1}) = 0. \tag{34d}$$

Note that due to the staggered grid (33a) and (34a) are calculated at $(m+\frac{1}{2}, n, k)$, (33b) and (34b) at $(m, n+\frac{1}{2}, k)$, (33c) and (34c) at (m,n) and (33d) and (34d) at (m,n,k).

3.4 Boundary conditions

Careful treatment of the boundary conditions is essential in order to avoid unwanted numerical phenomena, such as artificial boundary layers, unstable discretisations and numerical diffusion,

and to approximate the physical flow as well as possible. In this section we will start with the closed boundary conditions, followed by those for the open boundaries and finally we will deal with the boundary conditions at the bottom and the free surface. As an example the grid in Figure 2 is used. So, the closed boundaries are parallel to the x-axis and the open boundaries are parallel to the y-axis.

Closed Boundary conditions

For calculations on large scale problems, i.e. wide rivers and shallow seas, the impermeability of quays, dykes and dunes at the closed boundaries and the slip condition along these boundaries are supposed to have little effect on the velocities at the inner points. For several terms in the discretised equations the boundary conditions at the closed boundaries are not explicitly used, but the numerical approximations at points close to the boundaries are changed in accordance with them. A more detailed description of these changes is given below. In Figure 4 the horizontal grid along a closed boundary is given.

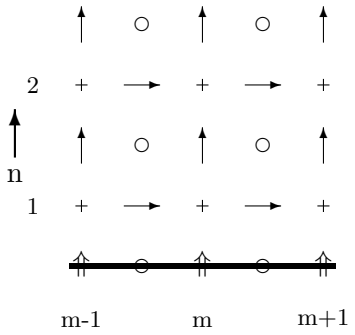

Figure 4. Horizontal grid along a closed boundary.

The horizontal advection term $v\frac{\partial v}{\partial y}$ is in practical sense not a large term near a closed boundary. However, when using the numerical discretisation for the derivative (as given in the previous section, item 5. in the list) it is possible that the numerical derivative is much larger. This is due to the fact that the numerical derivative is computed over two grid cells, of which the length, $2\triangle y$, is larger than the scale on which the boundary condition $v = 0$ actually has effect. This insight supports the choice to adjust the numerical approximations near the boundaries rather than explicitly use the boundary conditions at closed boundaries. Stelling (1984) proposed the following approximation for both stages:

$$v\frac{\partial v}{\partial y}\bigg|_{m,1\frac{1}{2}} \approx \begin{cases} 0, & \text{if} \quad v_{m,1\frac{1}{2}} > 0, \\ v_{m,1\frac{1}{2}}(v_{m,2\frac{1}{2}} - v_{m,1\frac{1}{2}})/\triangle y, & \text{if} \quad v_{m,1\frac{1}{2}} \leq 0. \end{cases}$$

Note that in the first case the approximation is zeroth order and in the second case it is first order accurate. The horizontal advection term $v\frac{\partial v}{\partial y}$ at $(m, 2\frac{1}{2})$ is also treated in special way in the first stage, when $v_{m,2\frac{1}{2}} > 0$. The numerical approximation is

$$v\frac{\partial v}{\partial y}\bigg|_{m,2\frac{1}{2}} \approx \begin{cases} v_{m,2\frac{1}{2}}(v_{m,2\frac{1}{2}} - v_{m,1\frac{1}{2}})/\triangle y, & \text{if} \quad v_{m,2\frac{1}{2}} > 0, \\ v_{m,2\frac{1}{2}}(-3v_{m,2\frac{1}{2}} + 4v_{m,3\frac{1}{2}} - v_{m,4\frac{1}{2}})/2\triangle y, & \text{if} \quad v_{m,2\frac{1}{2}} \leq 0. \end{cases}$$

In large scale problems the use of the free slip condition is allowed. For the horizontal advection term $v\frac{\partial u}{\partial y}$ the free slip condition, $\frac{\partial u}{\partial y} = 0$, and the impermeability condition, $v = 0$, support the

following approximations for the first stage:

$$v\frac{\partial u}{\partial y} \approx 0$$

and for the second stage:

$$v\frac{\partial u}{\partial y}\bigg|_{m+\frac{1}{2},1} \approx \begin{cases} 0, & \text{if} \quad \bar{v}_{m+\frac{1}{2},1} > 0, \\ \bar{v}_{m+\frac{1}{2},1}(-3u_{m+\frac{1}{2},1} + 4u_{m+\frac{1}{2},2} - u_{m+\frac{1}{2},3})/2\triangle y, & \text{if} \quad \bar{v}_{m+\frac{1}{2},1} \leq 0. \end{cases}$$

Note that the overbar on v indicates an averaged value as defined in Section 3.3. In the second stage the numerical approximation at $(m+\frac{1}{2}, 2)$ is replaced with:

$$v\frac{\partial u}{\partial y}\bigg|_{m+\frac{1}{2},2} \approx \begin{cases} \bar{v}_{m+\frac{1}{2},2}(u_{m+\frac{1}{2},2} - u_{m+\frac{1}{2},1})/\triangle y, & \text{if} \quad \bar{v}_{m+\frac{1}{2},2} > 0, \\ \bar{v}_{m+\frac{1}{2},2}(-3u_{m+\frac{1}{2},2} + 4u_{m+\frac{1}{2},3} - u_{m+\frac{1}{2},4})/2\triangle y, & \text{if} \quad \bar{v}_{m+\frac{1}{2},2} \leq 0. \end{cases}$$

The second order derivatives, $\nu^H \frac{\partial^2 u}{\partial y^2}$ and $\nu^H \frac{\partial^2 v}{\partial y^2}$, in the horizontal viscosity terms are approximated as follows near the closed the boundary:

$$\nu^H \frac{\partial^2 u}{\partial y^2}\bigg|_{m+\frac{1}{2},1} \approx \begin{cases} 0 & \text{in the first stage,} \\ \nu^H_{m+\frac{1}{2},1}(u_{m+\frac{1}{2},2} - u_{m+\frac{1}{2},1})/\triangle y^2 & \text{in the second stage,} \end{cases}$$

$$\nu^H \frac{\partial^2 v}{\partial y^2}\bigg|_{m,1\frac{1}{2}} \approx \begin{cases} \nu^H_{m,1\frac{1}{2}}(v_{m,\frac{1}{2}} - 2v_{m,1\frac{1}{2}} + v_{m,2\frac{1}{2}})/\triangle y^2 & \text{in the first stage,} \\ 0 & \text{in the second stage.} \end{cases}$$

Note that in the second formula the velocity component at the closed boundary ($v_{m,\frac{1}{2}}$) is explicitly taken into account, while this is avoided in the first formula. The second order derivatives with respect to x, $\nu^H \frac{\partial^2 u}{\partial x^2}$ and $\nu^H \frac{\partial^2 v}{\partial x^2}$, are approximated with second order accurate central difference schemes.

Boundary conditions on ζ at closed boundaries are only given if necessary. The derivative of ζ with respect to x in equations (33a) and (34a) does not imply the need for a boundary condition on ζ, because the closed boundaries are parallel to the x-axis. The derivative of ζ with respect to y, however, in the horizontal momentum equation in y-direction requires a boundary condition on ζ, but only in the second stage. It is obvious that the equations (34b) and (34c) are coupled. To solve these equations (34b) is substituted in (34c) leading to a tridiagonal system for ζ (see Section 3.5). Points near the closed boundary require data of points just beyond the boundary. The boundary condition $\frac{\partial \zeta}{\partial y} = 0$ satisfies this need.

Open boundary conditions

We recognise two types of open boundaries, namely inflow and outflow boundaries. At outflow boundaries non-reflective boundary conditions are preferred. For now, however, we will only use velocity and water level boundary conditions at inflow as well as outflow boundaries. At open boundaries only one type of boundary condition should be given. In Figure 5 the horizontal grid along an open boundary is given for both types of boundary conditions.

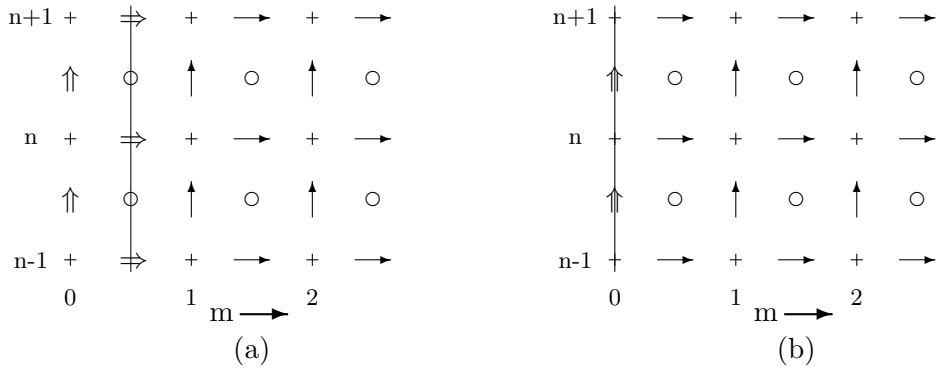

Figure 5. The horizontal grid along an open boundary for a velocity boundary condition (a) and for a water level boundary condition (b).

First we will discuss the velocity boundary condition. A velocity boundary condition can be a complete two-dimensional velocity profile or it can consist of a condition on the depth-integrated velocity along the border in combination with a vertical velocity profile. This vertical velocity profile is usually a logarithmic or uniform profile.

At inner points the horizontal advection term $u\frac{\partial u}{\partial x}$ in the first stage is approximated with a second order central difference scheme. Near the open velocity boundary as in Figure 5a this approximation does not cause any problems, so it remains unchanged. In the second stage this term is approximated as follows:

$$u\frac{\partial u}{\partial x}\bigg|_{1\frac{1}{2},n} \approx \begin{cases} u_{1\frac{1}{2},n}(u_{1\frac{1}{2},n} - u_{\frac{1}{2},n})/\triangle x, & \text{if} \quad u_{1\frac{1}{2},n} > 0, \\ u_{1\frac{1}{2},n}(-3u_{1\frac{1}{2},n} + 4u_{2\frac{1}{2},n} - u_{3\frac{1}{2},n})/2\triangle x, & \text{if} \quad u_{1\frac{1}{2},n} \leq 0. \end{cases}$$

At open boundaries the tangential velocity component is assumed to be zero. This corresponds with $v_{0,n} = 0\ \forall n$ for both types of boundary condition in Figure 5. The numerical approximation of the horizontal advection term $u\frac{\partial v}{\partial x}$ near open velocity boundaries for the first stage is:

$$u\frac{\partial v}{\partial x}\bigg|_{1,n+\frac{1}{2}} \approx \begin{cases} \bar{u}_{1,n+\frac{1}{2}}(v_{2,n+\frac{1}{2}} - v_{0,n+\frac{1}{2}})/2\triangle x, & \text{if} \quad \bar{u}_{1,n+\frac{1}{2}} > 0, \\ 0, & \text{if} \quad \bar{u}_{1,n+\frac{1}{2}} \leq 0 \end{cases}$$

and for the second stage:

$$u\frac{\partial v}{\partial x}\bigg|_{1,n+\frac{1}{2}} \approx \begin{cases} \bar{u}_{1,n+\frac{1}{2}}(v_{1,n+\frac{1}{2}} - v_{0,n+\frac{1}{2}})/\triangle x, & \text{if} \quad \bar{u}_{1,n+\frac{1}{2}} > 0 \\ \bar{u}_{1,n+\frac{1}{2}}(-3v_{1,n+\frac{1}{2}} + 4v_{2,n+\frac{1}{2}} - v_{3,n+\frac{1}{2}})/2\triangle x, & \text{if} \quad \bar{u}_{1,n+\frac{1}{2}} \leq 0. \end{cases}$$

The numerical approximations of the horizontal viscosity terms do not need a special treatment near open velocity boundaries and therefore they remain unchanged. For the same reasons as near closed boundaries a boundary condition on ζ is only given when necessary. In the first stage the boundary condition $\frac{\partial \zeta}{\partial x} = 0$ is used.

When a water level boundary condition is prescribed the numerical boundary is set along the ζ grid points (see Figure 5b). The numerical approximations near the open boundary of the various terms are different than with a velocity boundary condition. The numerical approximation of the horizontal advection term $u\frac{\partial u}{\partial x}$ at $(\frac{1}{2}, n)$ is replaced with

$$u\frac{\partial u}{\partial x}\bigg|_{\frac{1}{2},n} \approx \begin{cases} 0, & \text{if} \quad u_{\frac{1}{2},n} > 0, \\ u_{\frac{1}{2},n}(u_{1\frac{1}{2},n} - u_{\frac{1}{2},n})/\triangle x, & \text{if} \quad u_{\frac{1}{2},n} \leq 0 \end{cases}$$

for both stages. The horizontal advection term $u\frac{\partial v}{\partial x}$ is discretised near the open boundary according to a second order central scheme in the first stage:

$$u\frac{\partial v}{\partial x}\bigg|_{1,n+\frac{1}{2}} \approx \bar{u}_{1,n+\frac{1}{2}}(v_{2,n+\frac{1}{2}} - v_{0,n+\frac{1}{2}})/2\triangle x.$$

For the second stage either a zeroth order approximation or second order upwind scheme is used, depending on the flow direction of u. The approximation reads

$$u\frac{\partial v}{\partial x}\bigg|_{1,n+\frac{1}{2}} \approx \begin{cases} 0, & \text{if} \quad \bar{u}_{1,n+\frac{1}{2}} > 0, \\ \bar{u}_{1,n+\frac{1}{2}}(-3v_{1,n+\frac{1}{2}} + 4v_{2,n+\frac{1}{2}} - v_{3,n+\frac{1}{2}})/2\triangle x, & \text{if} \quad \bar{u}_{1,n+\frac{1}{2}} \leq 0. \end{cases}$$

The horizontal viscosity operator for u, $\nu^H \Delta u$, in the second stage is approximated as follows:

$$\nu^H \Delta u\big|_{1\frac{1}{2},n} \approx \nu^H_{1\frac{1}{2},n}(u_{1\frac{1}{2},n-1} - 2u_{1\frac{1}{2},n} + u_{1\frac{1}{2},n+1})/\triangle y^2.$$

The horizontal viscosity terms for v in the first stage are not treated in a special way. In both directions the second order difference schemes are used.

Bottom and surface boundary conditions

At the bottom as well as at the free surface three boundary conditions should be given for each of the velocity components. It is obvious that due to the impermeability of the bottom and the free surface the relative vertical velocity component ω is zero at these boundaries. Bottom friction and wind stresses at the free surface will provide the remaining boundary conditions. In Figure 6 the vertical grid along the free surface is given.

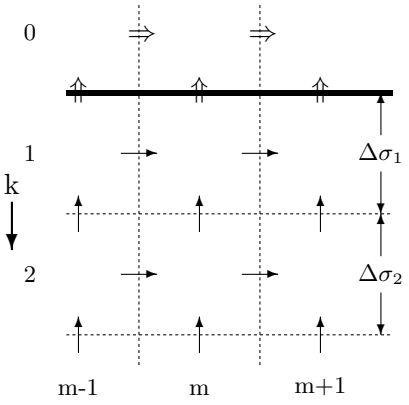

The arrow (⇑) indicates a Dirichlet boundary condition on the relative vertical velocity component. The other arrow (⇒) indicates a Neumann boundary condition on the horizontal velocity component.

Figure 6. Vertical grid along the free surface.

The Neumann boundary conditions for the wind stresses (see eqns. (23) and (24)) are only applied to the vertical viscosity terms $\frac{1}{H^2}\frac{\partial}{\partial\sigma}(\nu_t^V\frac{\partial u}{\partial\sigma})$ and $\frac{1}{H^2}\frac{\partial}{\partial\sigma}(\nu_t^V\frac{\partial v}{\partial\sigma})$ and not to the vertical advection terms $\frac{\omega}{H}\frac{\partial u}{\partial\sigma}$ and $\frac{\omega}{H}\frac{\partial v}{\partial\sigma}$. For the vertical advection terms at the surface first order upwind schemes are used as numerical approximations. For the velocity component in x-direction, u, at $(m+\frac{1}{2}, n)$ this reads

$$\frac{\omega}{H}\frac{\partial u}{\partial\sigma}\bigg|_{k=1} \approx \bar{\omega}_1 \frac{u_1 - u_2}{\frac{1}{2}(h_1 + h_2)}.$$

In the numerical approximation of the vertical viscosity terms two first order derivatives are subtracted (see list item 14 in section 3.3). Along the surface (when $k = 1$) one of these

derivatives equals the expression for wind stress, which accordingly replaces that derivative. The vertical viscosity term for u at the surface becomes

$$\frac{1}{H^2}\frac{\partial}{\partial\sigma}\left(\frac{\partial u}{\partial\sigma}\right)\bigg|_{k=1} \approx \frac{1}{h_1}\left[\frac{|\vec{\tau}_s|\cos\theta}{\rho} - \nu^V_{1\frac{1}{2}}\frac{u_1-u_2}{\frac{1}{2}(h_1+h_2)}\right].$$

The boundary conditions at the bottom (eqns. (21) and (22)) are treated equivalently.

3.5 Solution procedure

In this section we will explain the procedure of solving the discrete three-dimensional shallow-water equations. Only the first stage will be treated, since the procedure is equivalent for both stages. In this section we will adjust the indices for u, v and ω and only use whole numbers, so $v_{m,n}$ is $v_{m,n+\frac{1}{2}}$ and ω_k is $\omega_{k+\frac{1}{2}}$ for example. As a reminder we note that the number of grid cells in x-, y- and σ-direction are M, N and K, respectively.

First equation (33b), the momentum equation in y-direction, will be solved. The horizontal velocity v has been taken implicitly in all the terms of this equation. However, this results in a large banded matrix equation for $\underline{v}$. If the vector $\underline{v}$ is arranged in respectively the vertical and the horizontal (first in y- then in x-direction) directions, then the matrix has the following form:

$$\begin{pmatrix}
T_1 & D^{(1y)}_{12} & D^{(2y)}_{13} & \emptyset & \dots & \emptyset & D^{(1x)}_{1,N+1} & \emptyset & \dots & \emptyset & D^{(2x)}_{1,2N+1} & \emptyset & \\
D^{(-1y)}_{21} & T_2 & D^{(1y)}_{23} & D^{(2y)}_{24} & \emptyset & \dots & \emptyset & D^{(1x)}_{2,N+2} & \emptyset & \dots & \emptyset & D^{(2x)}_{2,2N+2} & \ddots \\
D^{(-2y)}_{31} & D^{(-1y)}_{32} & T_3 & D^{(1y)}_{34} & D^{(2y)}_{35} & \emptyset & \dots & \emptyset & D^{(1x)}_{3,N+3} & \emptyset & \dots & \emptyset & \ddots \\
\emptyset & D^{(-2y)}_{42} & D^{(-1y)}_{43} & T_4 & D^{(1y)}_{45} & D^{(2y)}_{46} & \emptyset & \dots & \emptyset & D^{(1x)}_{4,N+4} & \emptyset & \dots & \ddots \\
\emptyset & \emptyset & \ddots & \ddots & \ddots & \ddots & \ddots & & & & \ddots & &
\end{pmatrix}$$

where T_i is a tridiagonal matrix with the coefficients (if $i = (m-1)N+n$) for $v_{m,n,k}$ $\forall k$. $D^{(jy)}_{i,i+j}$ is a diagonal matrix with the coefficients for $v_{m,n+j,k}$ $\forall k$ with $i = (m-1)N+n$ and $j \in \{-2,-1,1,2\}$. $D^{(jx)}_{i,i+j\cdot N}$ is a diagonal matrix with the coefficients for $v_{m+j,n,k}$ $\forall k$ with $i = (m-1)N+n$ and $j \in \{-2,-1,1,2\}$. Note that $D^{(-2x)}$, $D^{(-2y)}$, $D^{(2y)}$ and $D^{(2x)}$ can have zeros on the diagonal due to the second order upwind schemes.

The band width of the matrix is too large to use a direct method. Therefore a Gauss-Jacobi iterative scheme is used in horizontal direction to solve this equation. In the vertical direction the implicit values are maintained, resulting in a tridiagonal matrix equation (only the coefficients in T_i remain). A single iteration is computed according to a red/black update. The red/black pattern is 'placed' horizontally. If we divide the vector $\underline{v}$ into $\underline{v}_1$, $\underline{v}_2$,..., $\underline{v}_{M\cdot N}$, then the first (red) of the two matrix equations to be solved reads

$$\begin{pmatrix}
T_1 & & & & \\
& T_3 & & & \\
& & \ddots & & \\
& & & T_{M\cdot N-3} & \\
& & & & T_{M\cdot N-1}
\end{pmatrix}
\begin{pmatrix}
\underline{v}_1 \\ \underline{v}_3 \\ \vdots \\ \underline{v}_{M\cdot N-3} \\ \underline{v}_{M\cdot N-1}
\end{pmatrix} = \underline{f}_1,$$

where $\underline{f}_1$ is the appropriate right hand side including all the variables, which are taken explicitly. The other (black) matrix equation is similar. The right hand side for this equation, however, is constructed using the latest calculated values for $\underline{v}_1, \underline{v}_3, ..., \underline{v}_{M\cdot N-1}$.

Combining both matrix equations (red and black), while taking in account the last remark, results in a matrix equation with a matrix of the form:

$$\begin{pmatrix} T_1 & \emptyset & \emptyset & \dots & \emptyset & \emptyset & \emptyset & \dots & & \\ D_{21}^{(-1y)} & T_2 & D_{23}^{(1y)} & \emptyset & \dots & \emptyset & D_{2,N+2}^{(1x)} & \emptyset & \dots & \\ \emptyset & \emptyset & T_3 & \emptyset & \emptyset & \dots & \emptyset & \emptyset & \emptyset & \dots \\ \emptyset & D_{42}^{(-2y)} & D_{43}^{(-1y)} & T_4 & D_{45}^{(1y)} & \emptyset & \dots & \emptyset & D_{4,N+4}^{(1x)} & \emptyset & \dots \\ \emptyset & \emptyset & \ddots & \ddots & \ddots & \ddots & \ddots & & & \ddots \end{pmatrix}$$

If the red/black pattern would be placed differently or if the main flow would be different, then this matrix would also be different. However, it is not expected that the result of the iteration would differ that much.

The equations (33a) and (33c) are coupled. In order to solve these equations, (33a) will be substituted in (33c). Therefore equation (33a) first has to be solved with respect to $u^{p+\frac{1}{2}}$. In general terms the discrete momentum equation in x-direction (33a) can be written as

$$A\underline{u}^{p+\frac{1}{2}} + B\underline{\zeta}^{p+\frac{1}{2}} = \underline{f}^{p}, \tag{35}$$

where $A \in \mathbb{R}^{MNK \times MNK}$ is a tridiagonal matrix consisting of MN smaller tridiagonal matrices $A_i \in \mathbb{R}^{K \times K}$. The matrix A_i holds the coefficients for $v_{m,n,k}$ $\forall k$ with $i = (1-m)N + n$. The matrix $B \in \mathbb{R}^{MNK \times (M+1)N}$ can be written as

$$B = \frac{g}{\triangle x} \begin{pmatrix} C & & & \\ & C & \emptyset & \\ & & \ddots & \\ & \emptyset & & C \\ & & & C \end{pmatrix} \quad \text{with} \quad C = \begin{pmatrix} -\underline{1} & \underline{1} & & & \\ & -\underline{1} & \underline{1} & & \emptyset \\ & & -\underline{1} & \underline{1} & \\ & \emptyset & & \ddots & \ddots \\ & & & & -\underline{1}\ \underline{1} \end{pmatrix},$$

where $\underline{1} \in \mathbb{R}^{K}$ is the vector with only ones. The vector $\underline{f}^{p}$ contains all the terms with only explicit variables. Due to the staggered grid the matrix C (and hence also B) is not square. Performing a Gaussian elimination process on (35) leads to

$$\underline{u}^{p+\frac{1}{2}} + B'\underline{\zeta}^{p+\frac{1}{2}} = \underline{f'}^{p}.$$

This procedure does not cause any fill-in in the matrix B, due to the fact that the matrix A consist of smaller tridiagonal matrices A_i. The depth-averaged form of this expression is needed in the continuity equation (33c) and can easily be calculated by multiplying every row with the accompanying relative layer thickness $\Delta\sigma_k$ and adding subsequent rows. This result in

$$\underline{U}^{p+\frac{1}{2}} + B''\underline{\zeta}^{p+\frac{1}{2}} = \underline{f''}^{p}$$

with $B'' \in \mathbb{R}^{MN \times (M+1)N}$ and $\underline{U} = \sum_k \Delta\sigma_k u_k$, the depth-averaged velocity component in x-direction.

Substituting this expression for $\underline{U}^{p+\frac{1}{2}}$ and the horizontal velocities in y-direction, $\underline{V}^{p}$, in (33c) leads to a tridiagonal system for $\underline{\zeta}^{p+\frac{1}{2}}$ in x-direction. Substituting the result of this equation into the expression for $\underline{u}^{p+\frac{1}{2}}$ gives the horizontal velocities in x-direction.

The depth-integrated continuity equation (33c) describes the level of the water surface ζ in the water column at coordinates (m, n) by calculating the net inflow in that column. It guarantees conservation of mass. It is important for this calculation that the term HU is taken either

completely implicit or completely explicit (the same restriction applies to HV). When this is not the case the numerical approximation is not mass conservative. For flow calculations this phenomenon is not so severe. However, when using non-mass-conservative calculated flow data in transport equations for a pollutant, for instance, some of the pollutant may disappear or appear.

When taking HU implicit, as done in (33c), then the equation will be non-linear. A way to deal with this problem is using an iterative scheme for $\underline{\zeta}^{p+\frac{1}{2}}$ (Kester and Stelling, 1992). The barotropic term $-g\,S_x(\zeta^{p+\frac{1}{2}})$ in equation (33a) is multiplied by $H^{p+\frac{1}{2},i}/H^{p+\frac{1}{2},i+1}$ (with $H^{p+\frac{1}{2},0} := H^p$). With this modification the equations (33a) and (33c) read respectively

$$\begin{aligned}\frac{u^{p+\frac{1}{2}}-u^p}{\tau/2} + u^{p+\frac{1}{2}}\,S_x(u^p) + v^{p+\frac{1}{2}}\,S_y(u^p) + \omega^p\,S_\sigma(u^{p+\frac{1}{2}}) \\ = -g\,\frac{H^{p+\frac{1}{2},i}}{H^{p+\frac{1}{2},i+1}}\,S_x(\zeta^{p+\frac{1}{2},i+1}) + S_{\sigma\sigma}(u^{p+\frac{1}{2}}) + f v^{p+\frac{1}{2}},\end{aligned} \tag{36a}$$

$$\frac{\zeta^{p+\frac{1}{2},i+1}-\zeta^p}{\tau/2} + S_x\left(H^{p+\frac{1}{2},i+1}\sum_k \Delta\sigma_k u_k^{p+\frac{1}{2}}\right) + S_y\left(H^p\sum_k \Delta\sigma_k v_k^p\right) = 0, \tag{36b}$$

where i denotes the current iterate. After the substitution of (36a) in (36b) as described above, a linear tridiagonal iterative system for $\underline{\zeta}^{p+\frac{1}{2}}$ arises, of which the result is substituted in (36a).

Finally, the continuity equation (33d) can be solved by substituting previous computed results. This equation is only used to derive the relative vertical velocity components, $\omega_{m,n,k}$. Note that there are at a horizontal coordinate (m,n) K continuity equations for $K-1$ unknown vertical velocity components. Therefore one of the equations is used for verification of the calculations.

4 Description of problem

In the course of years Delft3D-FLOW has been adjusted more than once in order to cope with unexpected results. However, some unwanted phenomena still remain. Sensitivity with respect to input parameters, compilers (and compiler options) and problem size is one of present interest. Computed problems demonstrate variable sensitivity. Different operating systems for instance (and thus different compilers) always give different results, which in some cases are significant. The size of the grid may cause another problem, namely the accumulative error due to large matrices.

The consequences of these kinds of inaccuracies may be rather severe. If a computed water level appears to be too low dykes may not be heightened while they should be. On the other hand, if it appears to be too high, much effort and money for heightening dykes may be wasted. The diffusion of a pollutant in rivers and seas are calculated using the results of Delft3D-FLOW. This diffusion would not be calculated well if the computed currents are fairly inaccurate.

4.1 Test cases

Test cases which demonstrate several of these sensitivities, will be used to illustrate and motivate our research. Below an overview of the test cases is given.

Test case 1: Reservoir with island and dams

In this test case (WL reference: '01-bakje') a square reservoir (8 by 8 km) with open boundaries is simulated. A square island is situated in the centre of the reservoir from which eight thin dams stretch out toward the boundaries, see Figure 7. At the open boundaries water level boundary conditions are prescribed. On all boundaries the homogeneous condition $\zeta = 0$ is imposed, except for the 'lower' boundary on which a tidal condition is defined.

In the lower corners high velocities occur in the current due to the small distance between the imposed homogeneous boundary condition and the tidal boundary condition, see Figure 7.

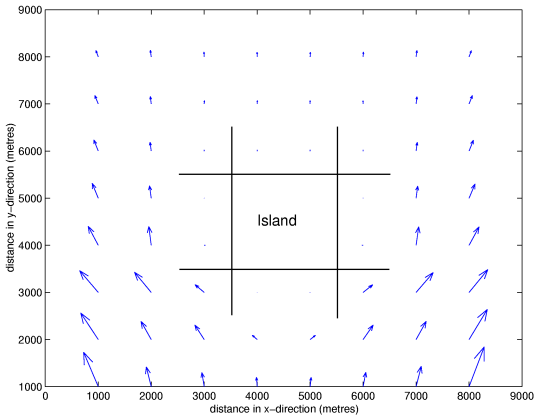

Figure 7. Vector field of the depth integrated velocity.

This test case has been simulated on four different operating systems. The results on the Windows and HP systems differ less than one percent. Comparison of the water levels computed on the Windows machine and the Sun Sparc machine shows differences up to 50%!

Test case 2: Reservoir with tidal condition

In this second test case (WL reference: '07-chezy') we simulate a rectangular reservoir (20 by 5 km) with closed boundaries along the long sides and open boundaries on the short sides. On one of the open boundaries the homogeneous water level condition is imposed and on the other open boundary a tidal condition is defined. The vertical grid is chosen counter-intuitively. The relative layer thickness, $\Delta\sigma_k$, is set to

$$0.01, 0.1, 0.09, 0.08, 0.06, 0.05, 0.04, 0.03, 0.02, 0.02, 0.03, 0.04, 0.05, 0.06, 0.08, 0.09, 0.1, 0.01$$

for $k = 1$ to $k = 20$ respectively. This results in rather peculiar flow data at certain points in time, see Figure 8. The vertical velocity component in this figure is scaled up by a factor of approximately 1000.

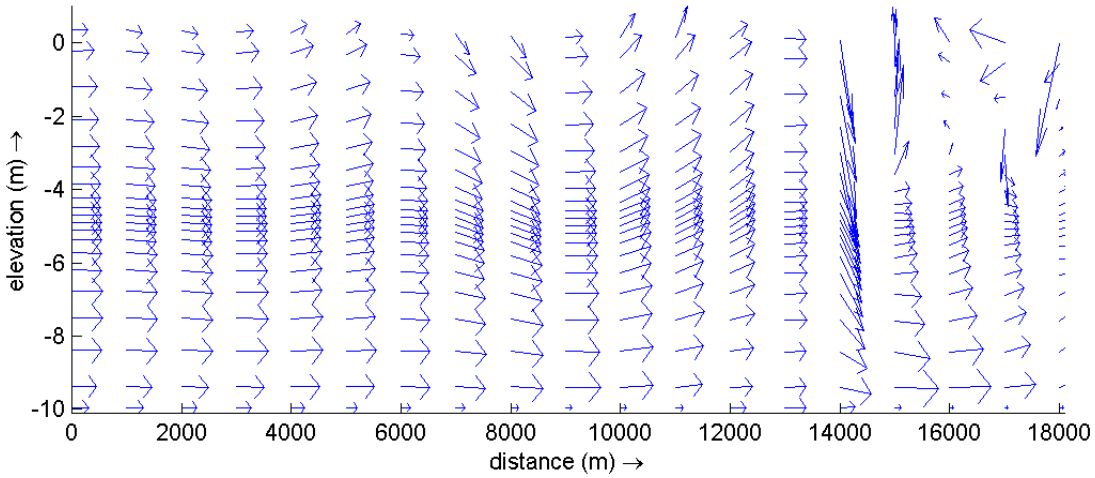

Figure 8. Cross-section of the velocity profile at a certain time step.

The peculiarities as shown in Figure 8 apparently occur at random and always near the 'eastern' boundary. A simulation where the relative layer thickness is equidistant shows no peculiarities besides the transient effects. Initial guesses are that the combination of the chosen σ-layers and the homogeneous, unnatural condition at that boundary are responsible for these curious results.

After the turn of the tide the main current changes direction. At several of these turns the velocity profile shows circular currents or relatively large vertical velocities. Again, when working with an equidistant layer thickness these results do not occur.

Test case 3: Navigational Channel

The navigational channel in a river or estuary is usually the deepest part of the water flow with the highest flow velocity. The water depth in the navigational channel may be up to 10 times larger than in other parts of the river or estuary. In this test case we will simulate a rectangular shaped reservoir with a straight and deep navigational channel. Does the bed topography has a negative effect on the condition numbers or the symmetry of the matrices? In other words, will instabilities occur?

In test case 5 we will simulate an existing geometry, namely the Westerschelde.

Test case 4: Long narrow reservoir

This test case is added in order to demonstrate how Delft3D-FLOW manages large geometries and thus large matrices. The reservoir is narrow but long (150 by 8 km). On the short open boundaries either water level or velocity boundary conditions are imposed. The long boundaries are 'closed'.

It is expected that due to the size of the problem rounding errors will accumulate during one time step. Furthermore we can swap the boundary conditions on both the open boundaries and compare those results with results computed before.

Test case 5: Westerschelde

The Westerschelde is an interesting test case, since the river bed is very uneven. At some points the water depth measures 40 metres, while at other points it is only a few meters. The width varies between three and six kilometres. This test case is in fact nothing more than a large, existing example of test case 3.

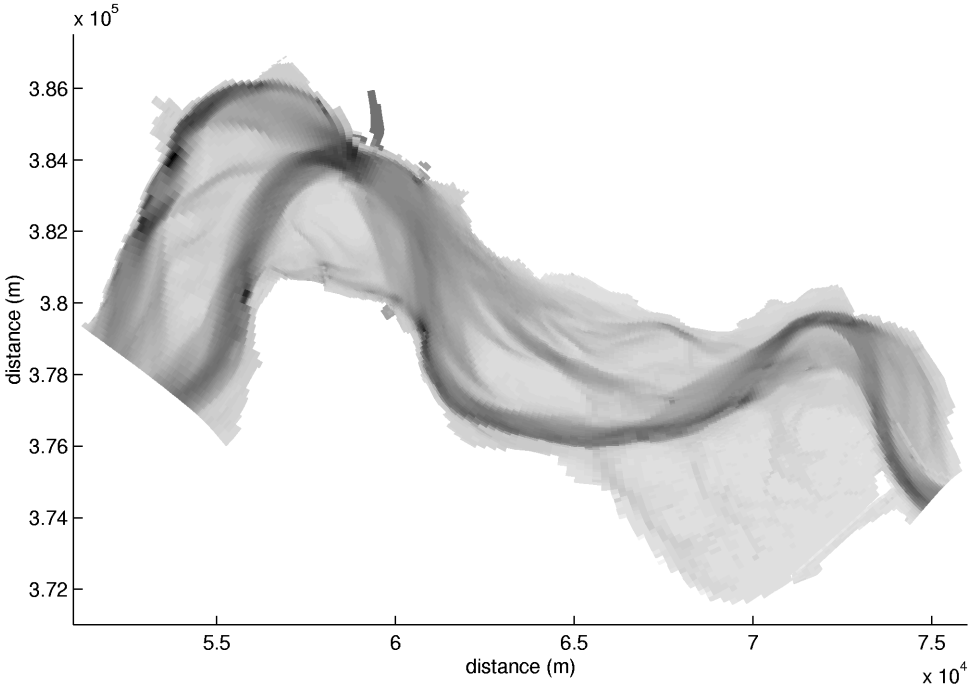

Figure 9. Bed topography of the Westerschelde.

4.2 Method of research

In the Fortran code of Delft3D-FLOW small additions have to be made in order to write out matrices and results. In Matlab this data can be used to compute residues and condition numbers of the matrices used.

To locate errors first several residues will be calculated. There are a number of residues which qualify for inspection.

The uncoupled momentum equations (33b) and (34a) are linear equations and solved with a Gauss-Seidel iterative scheme. For this iterative scheme not the residue but the difference between consecutive iterates is used in the stopping criterium. The residue is not necessarily very small.

The coupled momentum and continuity equations (33a) with (33c) and (34b) and (34c) are non-linear with respect to the water level ζ. The continuity equation is solved iteratively using a predetermined number of iterations. Thus also this residue may be considerably large.

Finally the residue of the discretised equations can be calculated by substituting the computed results. These residues are a result of all rounding and iterative errors made during one time step.

The numerical equations implemented in Delft3D-FLOW are supposed to be stable. So, erroneous results in one time step which are responsible for perturbed linear system in the next time step, are not expected to grow. The condition of the matrix in this system gives an idea how well the matrix equations are solved for a single time step

If the source of the irregularities is found, we will examine how they can be avoided.

References

AIAA, *Guide for the verification and validation of computational fluid dynamics simulations*, AIAA Guide G-077-1998 (Reston, VA, 1998).

Bijvelds, M., *Numerical modelling of estuarine flow over steep topography*, Ph.D. thesis, Delft University of Technology (Delft, 2001).

Jin, X.-Y., *Quasi-three-dimensional numerical modelling of flow and dispersion in shallow water*, Ph.D. thesis, Delft University of Technology (Delft, 1993).

Kester, J.A.Th.M. van and Stelling, G.S., 'Versnellen van TRISULA-3D', Delft Hydraulics Report Z81, WL | Delft Hydraulics (1992).

Launder, B.E. and Spalding, D., *Lectures in mathematical models of turbulence* (New York: Academic Press, 1972).

Mitchell, A.R. and Griffiths, D.F., *The Finite Difference Method in Partial Differential Equations*, pp. 59–70, 148–154 (New York: John Wiley, 1980).

Oberkampf, W.L. and Blottner, F.G., 'Issues in computational fluid dynamics code verification and validation', *AIAA Journal*, vol. 36, 687–695 (1998).

Phillips, N.G., 'A coordinate system having some special advantages for numerical forecasting', *Journal of Meteorology*, vol. 14, 184–185 (1957).

Rodi, W., 'Calculation of stably stratified shear-layer flows with a buoyancy-extended k-ϵ turbulence model', in Hunt, J.C.R. ed., *Turbulence and diffusion in stable environments*, pp. 111–140 (Oxford: Clarendon, 1985).

Stelling, G.S., *On the construction of computational methods for shallow water flow problems*, Ph.D. thesis, Delft University of Technology (Delft, 1984).

Uittenbogaard, R.E., Van Kester, J.A.Th.M. and Stelling, G.S., 'Implementation of three turbulence models in TRISULA for rectangular horizontal grids', Delft Hydraulics Report Z162, WL | Delft Hydraulics (Delft, 1992).

Wesseling, P., *Principles of Computational Fluid Dynamics*, Springer Series in Computational Mathematics, Vol.29 (Heidelberg: Springer, 2000).